PAPER

Online calibration method for SINS/LDV integrated navigation system based on left group error definition

To cite this article: Zhiyi Xiang *et al* 2024 *Meas. Sci. Technol.* **35** 055106

View the article online for updates and enhancements.

Online calibration method for SINS/LDV integrated navigation system based on left group error definition

Zhiyi Xiang[1,2] ⓘ**, Qi Wang**[1,2]**, Shilong Jin**[1,2]**, Xiaoming Nie**[1,2] **and Jian Zhou**[1,2,*] ⓘ

[1] College of Advanced Interdisciplinary Studies, National University of Defense Technology, Changsha 410073, People's Republic of China
[2] Nanhu Laser Laboratory, National University of Defense Technology, Changsha 410073, People's Republic of China

E-mail: wttzhoujian@163.com

CrossMark

Abstract

The integration of strapdown inertial navigation system (SINS) and laser Doppler velocimeter (LDV) is a reliable technology for land vehicle positioning. To ensure the best positioning performance of the SINS/LDV integrated navigation system, it is necessary to calibrate it accurately. However, the accuracy of the error model of the traditional calibration method is seriously affected by the large misalignment angle, which in turn affects the accuracy and consistency of the filtering, and eventually leads to the decline of the calibration accuracy. Therefore, this paper introduces the Lie group theory for the first time into the calibration study of the SINS/LDV integrated navigation system. Based on the error state vector defined by the left group error definition in the Lie group, the three calibration models of the SINS/LDV integrated navigation system are derived in the Earth-centered Earth-fixed frame, using velocity, displacement increment, and dead reckoning (DR) position, which are the three common observation information. The most significant advantage of these calibration models is their ability to handle large initial misalignment angles. The calibration models proposed in this paper are comprehensively evaluated by two long-distance vehicle experiments. The test results show that under normal conditions (no large attitude misalignment angle and all sensors are working properly), the Lie group-based calibration methods have similar performance to the traditional calibration method, but they have significant advantages in the case of large initial attitude deviation. In addition, using displacement increment and DR position as observations improves calibration performance compared to velocity.

Keywords: strapdown inertial navigation system (SINS), laser Doppler velocimeter (LDV), calibration, Lie group

1. Introduction

The integration of strapdown inertial navigation system (SINS) with laser Doppler velocimeter (LDV) is a promising scheme for land vehicles that require high positioning accuracy [1–4]. In SINS/LDV integrated navigation system, the SINS is the core navigation equipment, with advantages such as strong anti-jamming capability, high update frequency, and good concealment [5]. The LDV is used to provide high-precision velocity information, which has advantages such as high measurement accuracy, independence, non-contact measurement, fast dynamic response, good spatial resolution, wide range of velocity measurement, and high directional sensitivity [6]. Compared with the odometer (OD) currently widely used on land vehicles, the characteristics of the LDV non-contact measurement makes the measurement value of the LDV independent of the state of the

vehicle tire. This gives the LDV higher measurement accuracy and higher scale factor stability [7]. Moreover, for three-dimensional LDV, the non-contact measurement also enables the LDV measurement value to be unaffected by the vehicle sideslip.

For the SINS/LDV integrated navigation system, the accuracy of the reference velocity directly affects the positioning accuracy of the system. The reference velocity vector error consists of two components: the direction error and the module length error [8]. The direction error results from the misalignment angles between the LDV and the SINS, while the module length error, also known as the scale factor error, is mainly due to the deviation of the design value of the beam inclination angle of the LDV from the real value. The level arm between the LDV and the SINS is generally neglected because, unlike the OD which needs to be installed on the wheel, the LDV can be easily installed along with the inertial measurement unit (IMU) and the level arm can be easily obtained when the equipment is installed, and compensated through mathematical platform. In addition, the level arm-induced velocity error is usually small compared to the errors caused by the misalignment angles between the LDV and SINS as well as the scale factor error of the LDV. Therefore, in order to improve the positioning accuracy of the SINS/LDV integrated navigation system, it is necessary to calibrate the misalignment angles between the SINS and the LDV, as well as the scale factor error of LDV in advance. The least square method is a commonly used calibration method in SINS/Doppler velocity log (DVL) integrated navigation system, which can be divided into three calibration methods according to different observations: position observation, velocity observation and acceleration observation [9]. Zhang *et al* applied the least square method for the calibration of the SINS/LDV integrated navigation system, and proposed a calibration method based on the velocity observation without relying on any additional equipment or benchmarks [10]. In addition, the calibration method based on the trajectory similarity principle has been applied to some extent in the land integrated navigation system [11]. This method uses the similarity between the dead-reckoning (DR) trajectory and the true trajectory of the integrated navigation system to calibrate the installation misalignment angle between the IMU and the OD or LDV and the scale factor of the OD and LDV. However, this method is more suitable for high-precision SINS, because for low-precision SINS, the installation misalignment angle between sensors is no longer the main source of error. In recent years, the online calibration method based on Kalman filter has been widely used in integrated navigation system. Wu *et al* studied the feasibility of self-calibration of SINS/OD integrated navigation system using OD output and non-holonomic constraint (NHC) as velocity observation, and conducted observability analysis [12]. Similar applications can be found in [13–18]. In [19], the DR position of SINS/DVL was used as position observations integrated with SINS. Combining Kalman filter with other optimal estimation methods is also a reliable calibration mode. Xiang *et al* proposed an online calibration method for SINS/LDV integrated navigation system based on position observation, which combines Kalman filter with Davenport's

q-method, and verified the effectiveness and robustness of the method through experiments [20].

For the online calibration method of SINS/LDV integrated navigation system using Kalman filter, the calibration performance can be improved from three aspects: filtering algorithm, measurement model and process model. Filtering algorithms are generally universal, so the online calibration of SINS/LDV integrated navigation system can directly use the existing classical or advanced filtering algorithms, which mainly aim to suppress unknown noise and outliers in the sensor. Since the most widely used measurements in SINS/LDV integrated navigation system is the body velocity of the vehicle, the measurement models in the calibration process of SINS/LDV integrated navigation system are divided into velocity observation model based on LDV velocity output, displacement incremental observation model based on LDV velocity integration, and position observation model based on SINS/LDV DR position output. As for the process model in the calibration process of SINS/LDV integrated navigation system, the existing calibration methods of SINS/LDV and SINS/OD integrated navigation system adopt the navigation frame SINS mechanization and the corresponding navigation frame error model. However, this model has some limitations, such as: the attitude error in the error model is defined on the manifold with small value assumption and the velocity error and position error are defined in Euclidean space, which makes the process model linear and only applicable to the case of small attitude error; the model is not independent of navigation parameters, so the navigation errors caused by the motion state of the vehicle and the errors of the sensor will seriously affect the accuracy of the model, and then affect the calibration accuracy of the integrated navigation system [21].

To alleviate the inconsistency of the coordinate system of the velocity error vector caused by specific force in the traditional process model, Scherzinger proposed a new velocity error transformation, and Wang *et al* developed the state transformation extended Kalman filter based on this idea [22–24]. Recently, the Lie group theory has been introduced in some inertial navigation fields [25–32]. The group of double direct spatial isometries $SE_3(3)$ is introduced to formulate the attitude matrix, velocity vector, and position vector into a group. If the corresponding dynamic model satisfies the 'group affine' property, a new state-independent linear error model can be obtained by using the mapping relationship between Lie groups and Lie algebra, and the state transition matrix of the error model is completely independent of the navigation parameters such as attitude, velocity and position. Through this model, the consistency of filtering can be well guaranteed. Chang *et al* [33] shows that by introducing an auxiliary velocity, the mechanization of SINS in the earth-centered earth-fixed (ECEF) frame satisfies the 'group affine' property with group state on $SE_3(3)$. The obtained left and right-invariant error state models are trajectory-independent, and their log-linearity, an advantage, makes them very suitable for attitude initialization with arbitrary misalignment. Tang *et al* [34] shows that for SINS/DVL integration using the error state model proposed in [33], the left-invariant error definition is more suitable for SINS/DVL navigation when considering

IMU bias. Chang *et al* [35] incorporates the DR position of the SINS/DVL integration with the attitude, velocity, and position computed by SINS as the elements of the group of triple direct isometries $SE_3(3)$. Based on the left-invariant error definition, it derives the corresponding error state model. Although this model no longer satisfies the group affine property after adding the DR position of SINS/DVL, [35] proves that it is still applicable in the case of large initial attitude misalignment. Although Lie group theory has been applied in SINS/OD integrated navigation and SINS/DVL integrated navigation and has improved the performance of the integrated navigation system to some extent. However, in these studies, the scale factor error of external velocity sensors and the installation misalignment angle between external velocity sensors and SINS have not been considered. The current calibration methods of these errors are still based on the traditional process model and measurement model.

This paper applies the Lie group theory to calibrate the SINS/LDV integrated navigation system. It derives the SINS/LDV calibration model based on Lie group $SE_2(3)$ in the ECEF frame, which includes two measurement models: velocity and displacement increment. It then uses the SINS/LDV DR position, which belongs to the left invariant observation, as the measurements of the calibration system, and formulates the DR position of SINS/LDV as elements of the Lie group $SE_3(3)$, along with the attitude, velocity, and position calculated by SINS. It also derives the SINS/LDV calibration model based on Lie group $SE_3(3)$ in the ECEF frame. Finally, it validates the effectiveness of the proposed calibration method through two vehicle-mounted experiments. Compared with previous calibration methods for the SINS/LDV integrated navigation system, the main contributions of this paper are as follows: (1) the Lie group theory is used to calibrate the SINS/LDV integrated navigation system. The linear error state-space models for SINS/LDV integration considering the error of LDV scale factor and the installation misalignment angle between IMU and LDV are derived based on the left invariant error definitions of $SE_2(3)$ and $SE_3(3)$; (2) based on the left invariant error definitions of $SE_2(3)$ and $SE_3(3)$, the measurement models for three kinds of observation information, namely velocity, displacement increment and DR position, are derived. Then, the performance of calibration models using different observation models is analyzed and compared; (3) the effectiveness of the calibration methods proposed in this paper is evaluated by comparing it with traditional calibration method. The Lie group-based calibration method shows a significant improvement over the traditional calibration method at large misalignment angles.

The rest of this paper is organized as follows. Section 2 introduces the traditional calibration model for SINS/LDV integrated navigation system. In section 3, the SINS/ LDV calibration model based on Lie group $SE_2(3)$ is proposed. In section 4, the SINS/LDV calibration model based on Lie group $SE_3(3)$ is proposed. In section 5, the proposed calibration models are compared with the traditional calibration model by using the vehicle-mounted field test data collected from LDV-aided SINS. Concluding remarks are given in section 6.
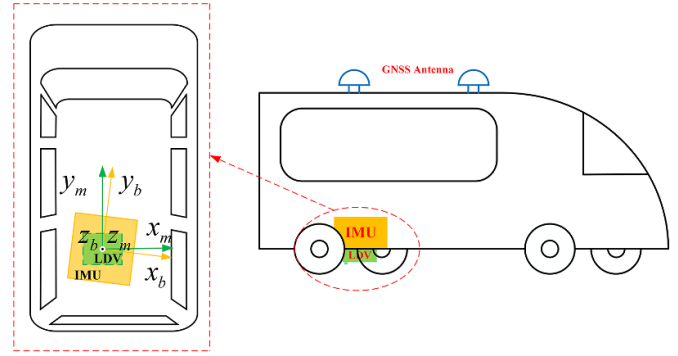
Figure 1. Installation relationship between the LDV, IMU and GNSS.

2. Review of SINS/LDV traditional calibration model

The installation relationship between the LDV, IMU and GNSS is shown in figure 1. The LDV body frame, denoted by the *m* frame, is defined as right-forward-upward. The IMU body frame, denoted by the *b* frame, is also defined as right-forward-upward. The navigation frame is defined as east-north-up and is denoted by the *n* frame. The ECEF frame is denoted by the *e* frame, which is located at the center of the earth and rotates with the earth. The inertial non-rotating frame is denoted by the *i* frame, which remains stationary with respect to the inertial space.

The optical path structure of the pitch-independent LDV system is shown in figure 2. θ_1 and θ_2 are the designed inclination angles of the two beams of LDV. υ_{LDV} denotes the velocity of the vehicle measured by pitch-independent LDV, which is given by the following equation [36]:

$$\upsilon_{\text{LDV}} = \frac{\lambda f_{\text{beam1}}}{2} \sqrt{1 + \left(\frac{1}{\tan(2\Delta\theta)} - \frac{1}{\sin(2\Delta\theta)} \frac{f_{\text{beam2}}}{f_{\text{beam1}}} \right)^2} \tag{1}$$

where λ is the wavelength of the laser, f_{beam1} and f_{beam2} are the Doppler frequencies measured by two beams, $\Delta\theta = \frac{\theta_2 - \theta_1}{2}$.

Since υ_{LDV} is only the forward velocity of the vehicle, it is necessary to obtain the three-dimensional velocity of the land vehicle with the help of the well-known NHC, and the vehicle velocity obtained by LDV in the *m* frame can be expressed as

$$\boldsymbol{\upsilon}_{\text{LDV}}^m = \begin{bmatrix} 0 & \upsilon_{\text{LDV}} & 0 \end{bmatrix}^T = (1 + \delta K) \boldsymbol{\upsilon}^m \tag{2}$$

where υ^m is the true velocity of the vehicle in the *m* frame, δK denotes the scale factor error due to the deviation of the beam inclination.

According to (2), the velocity obtained by LDV in the *n* frame is given as follows

$$\boldsymbol{\upsilon}_{\text{LDV}}^n = \tilde{\boldsymbol{C}}_b^n \boldsymbol{C}_m^b \boldsymbol{\upsilon}_{\text{LDV}}^m = (\boldsymbol{I}_3 - \boldsymbol{\varphi} \times) \boldsymbol{C}_b^n (\boldsymbol{I}_3 - \boldsymbol{\phi}_m \times) (1 + \delta K) \boldsymbol{\upsilon}^m \tag{3}$$

where $\boldsymbol{C}_b^n$ and $\tilde{\boldsymbol{C}}_b^n$ are the true and error-contaminated attitude matrices from the *b* frame to the *n* frame, respectively.
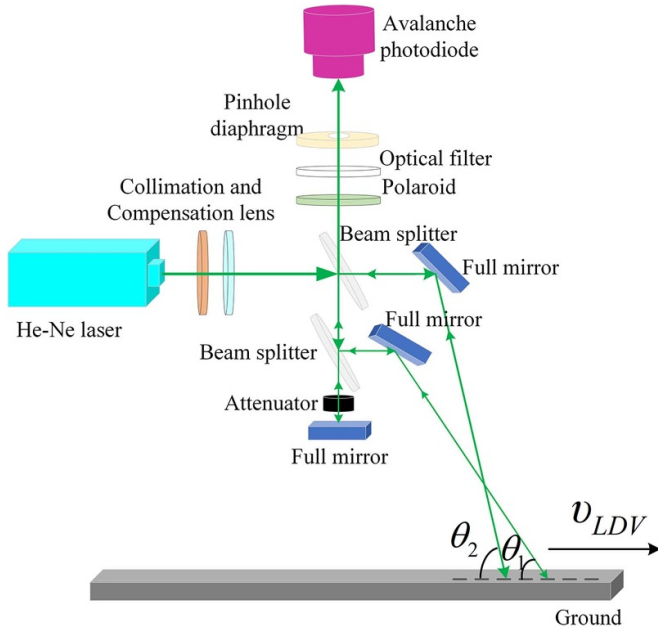
Figure 2. Optical schematic of the pitch-independent LDV.

I_3 denotes the 3×3 identity matrix, φ denotes the attitude error of the SINS. $(\cdot)\times$ means to solve the antisymmetric matrix. ϕ_m is the installation misalignment angles between the m frame and the b frame, $\phi_m = \begin{bmatrix} \phi_{mx} & \phi_{my} & \phi_{mz} \end{bmatrix}^T$, where ϕ_{mx}, ϕ_{my}, and ϕ_{mz} are the misalignment angles of pitch, roll, and heading, respectively.

According to (3), by omitting small quantities of the higher orders, the velocity error model of the LDV is given as

$$\delta \boldsymbol{v}^n_{\mathrm{LDV}} \approx (\boldsymbol{v}^n \times)\boldsymbol{\varphi} + \boldsymbol{C}^n_b(\boldsymbol{v}^m \times)\phi_m + \delta K \boldsymbol{v}^n. \quad (4)$$

For the traditional SINS/LDV online calibration system, the SINS error dynamics are as follows

$$
\begin{cases}
\dot{\boldsymbol{\varphi}} = \boldsymbol{\varphi} \times \boldsymbol{\omega}^n_{in} + \delta\boldsymbol{\omega}^n_{in} - \boldsymbol{C}^n_b \boldsymbol{\varepsilon}^b_{ib} \\
\delta\dot{\boldsymbol{v}}^n_{\mathrm{SINS}} = -\boldsymbol{\varphi} \times \boldsymbol{f}^n + \delta\boldsymbol{v}^n_{\mathrm{SINS}} \times (2\boldsymbol{\omega}^n_{ie} + \boldsymbol{\omega}^n_{en}) \\
\qquad\quad + \boldsymbol{v}^n_{\mathrm{SINS}} \times (2\delta\boldsymbol{\omega}^n_{ie} + \delta\boldsymbol{\omega}^n_{en}) + \boldsymbol{C}^n_b \boldsymbol{\nabla}^b_{ib} \\
\delta\dot{L} = \delta v_N / (R_M + h) - v_N \delta h \big/ (R_M + h)^2 \\
\delta\dot{\lambda} = \sec L \delta v_E / (R_N + h) + v_E \tan L \sec L \delta L / (R_N + h) \\
\qquad\quad - v_E \sec L \delta h \big/ (R_N + h)^2 \\
\delta\dot{h} = \delta v_U \\
\dot{\boldsymbol{\varepsilon}}^b_{ib} = \mathbf{0}_{3\times1} \\
\dot{\boldsymbol{\nabla}}^b_{ib} = \mathbf{0}_{3\times1}
\end{cases}
\quad (5)
$$

where $\boldsymbol{v}^n_{\mathrm{SINS}} = \begin{bmatrix} v_E & v_N & v_U \end{bmatrix}^T$ and $\delta\boldsymbol{v}^n_{\mathrm{SINS}} = \begin{bmatrix} \delta v_E & \delta v_N & \delta v_U \end{bmatrix}^T$ are the velocity and velocity error of SINS, respectively; $\delta\boldsymbol{p}_{\mathrm{SINS}} = \begin{bmatrix} \delta L & \delta\lambda & \delta h \end{bmatrix}^T$ denotes position error vectors of SINS; R_M and R_N are the principal radius of curvature of the prime meridian and the equator, respectively; L, λ, and h are the local latitude, local longitude,

and local altitude, respectively; $\boldsymbol{f}^n$ denotes the specific force output from accelerometers in the n frame; $\boldsymbol{\omega}^n_{in}$, $\boldsymbol{\omega}^n_{en}$ and $\boldsymbol{\omega}^n_{ie}$ are the rotation angular rate vectors of the n frame relative to the i frame, the n frame relative to the e frame, and the e frame relative to the i frame, respectively, and all vectors are projected in the n frame; $\boldsymbol{\varepsilon}^b_{ib}$ and $\boldsymbol{\nabla}^b_{ib}$ denote the gyro constant bias and the accelerometer constant bias, respectively; $\mathbf{0}_{3\times1}$ denotes the 3×1 zero vector.

Since the lasers inside the LDV usually have excellent performance and the installation relationship between the LDV and the SINS is fixed, the scale factor error of the LDV and the installation misalignment angle between the LDV and the SINS can be modeled as random constants, and the corresponding error equations of LDV are expressed as follows

$$
\begin{aligned}
\delta\dot{K} &= 0 \\
\dot{\phi}_{mx} &= 0. \\
\dot{\phi}_{mz} &= 0
\end{aligned}
\quad (6)
$$

It should be noted that ϕ_{my} has no effect on the performance of the SINS/1D-LDV integrated navigation system, it is unobservable and should be disregarded in this paper.

According to (5) and (6), the error state equation of the traditional SINS/ LDV calibration system is:

$$
\dot{\boldsymbol{x}} = \begin{bmatrix} \boldsymbol{F}_{\mathrm{SINS}} & \mathbf{0}_{15\times3} \\ \mathbf{0}_{3\times15} & \mathbf{0}_{3\times3} \end{bmatrix} \boldsymbol{x} + \begin{bmatrix} -\boldsymbol{C}^n_b & \mathbf{0}_{3\times3} \\ \mathbf{0}_{3\times3} & \boldsymbol{C}^n_b \\ \mathbf{0}_{12\times3} & \mathbf{0}_{12\times3} \end{bmatrix} \boldsymbol{w} \quad (7)
$$

where $\boldsymbol{F}_{\mathrm{SINS}}$ is a 15×15 state transition matrix based on (5), $\boldsymbol{w}$ denotes the system noise vector, and $\boldsymbol{x}$ is an 18-dimensional error state vector defined as:

$$
\begin{aligned}
\boldsymbol{x} &= \begin{bmatrix} \boldsymbol{x}_{\mathrm{SINS}} & \boldsymbol{x}_{\mathrm{LDV}} \end{bmatrix}^T \\
\boldsymbol{x}_{\mathrm{SINS}} &= \begin{bmatrix} \boldsymbol{\varphi}^T & \delta(\boldsymbol{v}^n_{\mathrm{SINS}})^T & \delta\boldsymbol{p}^T_{\mathrm{SINS}} & (\boldsymbol{\varepsilon}^b_{ib})^T & (\boldsymbol{\nabla}^b_{ib})^T \end{bmatrix}^T. \\
\boldsymbol{x}_{\mathrm{LDV}} &= \begin{bmatrix} \phi_{mx} & \phi_{mz} & \delta K \end{bmatrix}^T
\end{aligned}
\quad (8)
$$

The measurement equation of the traditional SINS/ LDV calibration system is

$$
\begin{aligned}
\boldsymbol{z} &= \begin{bmatrix} \boldsymbol{v}^n_{\mathrm{SINS}} - \boldsymbol{v}_{\mathrm{GNSS}} \\ \boldsymbol{p}_{\mathrm{SINS}} - \boldsymbol{p}_{\mathrm{GNSS}} \\ \boldsymbol{v}^n_{\mathrm{LDV}} - \boldsymbol{v}_{\mathrm{GNSS}} \end{bmatrix} \approx \begin{bmatrix} \delta\boldsymbol{v}^n_{\mathrm{SINS}} \\ \delta\boldsymbol{p}_{\mathrm{SINS}} \\ \delta\boldsymbol{v}^n_{\mathrm{LDV}} \end{bmatrix} = \boldsymbol{Hx} + \boldsymbol{v} \\
&= \begin{bmatrix} \mathbf{0}_{6\times3} & \boldsymbol{I}_6 & \mathbf{0}_{6\times6} & \mathbf{0}_{6\times2} & \mathbf{0}_{6\times1} \\ \boldsymbol{v}^n\times & \mathbf{0}_{3\times6} & \mathbf{0}_{3\times6} & \boldsymbol{C}^n_b \boldsymbol{C}_v & \boldsymbol{v}^n \end{bmatrix} \boldsymbol{x} + \boldsymbol{v}
\end{aligned}
\quad (9)
$$

where $\boldsymbol{H}$ is the measurement transition matrix, $\boldsymbol{v}$ is the measurement noise (zero-mean Gaussian white noise), $\boldsymbol{z}$ is the measurement value. $\boldsymbol{v}_{\mathrm{GNSS}}$ and $\boldsymbol{p}_{\mathrm{GNSS}}$ are the velocity and position outputs of the GNSS. $\boldsymbol{C}_v = \begin{bmatrix} 0 & \boldsymbol{v}^m_{(z)} & -\boldsymbol{v}^m_{(y)} \\ \boldsymbol{v}^m_{(y)} & -\boldsymbol{v}^m_{(x)} & 0 \end{bmatrix}^T$

3. The SINS/ LDV calibration model based on Lie group $SE_2(3)$

For the traditional SINS/LDV online calibration system, (5) shows that the various errors of SINS are coupled with each other, and its state transition matrix depends on the navigation parameters, such as attitude, velocity, position. When one of them has a large error, especially the attitude error, the accuracy of its error model will be seriously affected, which in turn affects the accuracy and consistency of the filtering. Moreover, (9) shows that the measurement transition matrix depends on C_b^n, v^n and v^m. This implies that the attitude accuracy of the calibration system will have a significant impact on the calibration results. If the process model and measurement model of the SINS/LDV online calibration system are trajectory-independent and its error propagation is autonomous, then the SINS/LDV online calibration system can recover faster from large errors caused by disturbances or outliers. To achieve this, the online calibration method based on Lie group $SE_2(3)$ and GNSS for the SINS/LDV integrated navigation system is proposed in this section.

3.1. Matrix Lie group and Lie algebra

A Lie group is a smooth manifold that obeys the group properties so that the group operations are smooth. The tangent space at the identity element of a Lie group has a natural Lie algebra structure, and this Lie algebra gives the local structure of the Lie group through the exponential map. In integrated navigation, the vehicle's attitude, velocity, and position are the three quantities of interest. They can be embedded as the element of the Lie group $SE_2(3)$ (also called the group of double direct isometrics):

$$SE_2(3) = \left\{ \chi = \begin{bmatrix} C & v & p \\ \mathbf{0}_{1\times3} & 1 & 0 \\ \mathbf{0}_{1\times3} & 0 & 1 \end{bmatrix} \in \mathbb{R}^{5\times5} \middle| \begin{array}{c} C \in SO(3) \\ v, p \in \mathbb{R}^3 \end{array} \right\}$$
(10)

where χ is a 5×5 matrix, including the attitude rotation matrix C and two three-dimensional vectors (the velocity vector v and the position vector p). $SO(3)$ denotes the special orthogonal group.

The inverse of a group matrix χ, is also a Lie group $SE_2(3)$; that is

$$\chi^{-1} = \begin{bmatrix} C^T & -C^T v & -C^T p \\ \mathbf{0}_{1\times3} & 1 & 0 \\ \mathbf{0}_{1\times3} & 0 & 1 \end{bmatrix} \in SE_2(3).$$
(11)

The Lie algebra $se_2(3)$ associated with $SE_2(3)$ and the exponential mapping from the Lie algebra to the corresponding Lie group are given as:

$$se_2(3) = \left\{ \boldsymbol{\xi}^\wedge = \begin{bmatrix} \boldsymbol{\theta} \times & v & p \\ \mathbf{0}_{1\times3} & 0 & 0 \\ \mathbf{0}_{1\times3} & 0 & 0 \end{bmatrix} \in \mathbb{R}^{5\times5} \right.$$
$$\left. \times \middle| \begin{array}{c} \boldsymbol{\xi} = \begin{bmatrix} \boldsymbol{\theta} & v & p \end{bmatrix}^T \in \mathbb{R}^9 \\ \boldsymbol{\theta}, v, p \in \mathbb{R}^3 \end{array} \right\}$$
(12)

$$\chi = \exp(\boldsymbol{\xi}) = \exp_m(\boldsymbol{\xi}^\wedge) = \sum_{k=0}^{\infty} \frac{1}{k!} (\boldsymbol{\xi}^\wedge)^k$$
$$= \begin{bmatrix} \exp_m(\boldsymbol{\theta}\times) & Jv & Jp \\ \mathbf{0}_{1\times3} & 1 & \\ \mathbf{0}_{1\times3} & & 1 \end{bmatrix}$$
(13)

where $(\bullet)^\wedge$ denotes the linear operation, $\boldsymbol{\theta}$ is the rotation vector, $\exp_m$ denotes the matrix exponential operation, and J is the left Jacobian matrix of $SO(3)$, which is given by

$$J = \sum_{k=0}^{\infty} \frac{1}{(k+1)!} (\boldsymbol{\theta}\times)^k$$
$$= \frac{\sin\theta}{\theta} I_3 + \left(1 - \frac{\sin\theta}{\theta}\right) aa^T + \frac{1-\cos\theta}{\theta} (a\times)$$
(14)

where $\theta = |\boldsymbol{\theta}|$ denotes the angle of rotation and $a = \frac{\boldsymbol{\theta}}{\theta}$ is the unit-length axis of rotation.

For a comprehensive introduction to Lie group theory, refer to [37].

3.2. Process model

The traditional SINS mechanization in the *e* frame is given as follows:

$$\dot{C}_b^e = C_b^e (\boldsymbol{\omega}_{ib}^b\times) - (\boldsymbol{\omega}_{ie}^e\times) C_b^e$$
$$\dot{v}_{eb}^e = C_b^e f^b - 2(\boldsymbol{\omega}_{ie}^e\times) v_{eb}^e + g^e$$
$$\dot{p}_{eb}^e = v_{eb}^e$$
(15)

where C_b^e denotes the direction cosine matrices from *b* frame to *e* frame; $\boldsymbol{\omega}_{ib}^b$ is the body angular rate measured by the gyroscopes in the *b* frame; $\boldsymbol{\omega}_{ie}^e$ denotes the rotation rate vector of earth; f^b is the specific force measured by accelerometers in the *b* frame; v_{eb}^e denotes the ground velocity in the *e* frame; g^e is the gravity vector; p_{eb}^e is the position vector in the *e* frame.

References [38] and [39] introduce an auxiliary velocity based on SINS mechanization into the *e* frame, which enables SINS mechanization to satisfy the group affine property. The auxiliary velocity is given by

$$v_{ib}^e = v_{eb}^e + \boldsymbol{\omega}_{ie}^e \times p_{eb}^e.$$
(16)

By introducing an auxiliary velocity vector, the (15) can be rewritten as follows:

$$\dot{C}_b^e = C_b^e (\boldsymbol{\omega}_{ib}^b\times) - (\boldsymbol{\omega}_{ie}^e\times) C_b^e$$
$$\dot{v}_{ib}^e = C_b^e f^b - \boldsymbol{\omega}_{ie}^e \times v_{ib}^e + G^e$$
$$\dot{p}_{eb}^e = v_{ib}^e - \boldsymbol{\omega}_{ie}^e \times p_{eb}^e$$
(17)

where G^e is the gravitational vector and is given by:

$$G^e = g^e + (\boldsymbol{\omega}_{ie}^e\times)^2 p_{eb}^e.$$
(18)

It should be noted that $p_{eb}^e = p_{ib}^e$, because according to the definition of the *e* frame and the earth-centered *i* frame, they have the same origin, and for navigation on earth, the body position relative to the earth-centered *i* frame, expressed in *e*

frame, and the body position relative to the *e* frame, expressed in *e* frame, are the same.

Formulating C_b^e, $\boldsymbol{v}_{ib}^e$ and $\boldsymbol{p}_{eb}^e$ as elements of Lie group $SE_2(3)$

$$\boldsymbol{\chi} = \begin{bmatrix} C_b^e & \boldsymbol{v}_{ib}^e & \boldsymbol{p}_{eb}^e \\ \mathbf{0}_{1\times3} & 1 & 0 \\ \mathbf{0}_{1\times3} & 0 & 1 \end{bmatrix} \tag{19}$$

$$\boldsymbol{\chi}^{-1} = \begin{bmatrix} C_e^b & -C_e^b\boldsymbol{v}_{ib}^e & -C_e^b\boldsymbol{p}_{eb}^e \\ \mathbf{0}_{1\times3} & 1 & 0 \\ \mathbf{0}_{1\times3} & 0 & 1 \end{bmatrix}. \tag{20}$$

For Lie group matrix, two different definitions of error can be used, namely, left-invariant error and right-invariant error. Given a Lie group matrix $\boldsymbol{\chi}$ and its inverse matrix $\boldsymbol{\chi}^{-1}$, the left and right invariant errors can be defined as $\boldsymbol{\eta} = \tilde{\boldsymbol{\chi}}^{-1}\boldsymbol{\chi}$ and $\boldsymbol{\eta} = \boldsymbol{\chi}\tilde{\boldsymbol{\chi}}^{-1}$ respectively.

For SINS/LDV online calibration system, the GNSS can provide accurate velocity and position information. The observation of GNSS can be given by

$$\boldsymbol{z}_{\text{GNSS},1} = \boldsymbol{v}_{\text{GNSS}}^e + \boldsymbol{\omega}_{ie}^e \times \boldsymbol{p}_{\text{GNSS}}^e \tag{21}$$

$$\boldsymbol{z}_{\text{GNSS},2} = \boldsymbol{p}_{\text{GNSS}}^e \tag{22}$$

where $\boldsymbol{v}_{\text{GNSS}}^e$ and $\boldsymbol{p}_{\text{GNSS}}^e$ are the outputs of the GNSS in the *e* frame for velocity and position, respectively.

According to [33], it is easy to see that the observation in (21) and (22) is a left-invariant observation for the group state (19). Moreover [34], demonstrates that for SINS/ external velocity sensors integration, the measurement of body velocity is neither left- nor right-invariant observation for the group state (19), but the left-invariant error definition is more suitable when considering IMU bias. Therefore, in the online calibration method based on Lie group $SE_2(3)$ and GNSS for the SINS/LDV integrated navigation system, the left-invariant group error is used

$$\begin{aligned} \boldsymbol{\eta} = \tilde{\boldsymbol{\chi}}^{-1}\boldsymbol{\chi} &= \begin{bmatrix} \tilde{C}_e^b C_b^e & \tilde{C}_e^b(\boldsymbol{v}_{ib}^e - \tilde{\boldsymbol{v}}_{ib}^e) & \tilde{C}_e^b(\boldsymbol{p}_{eb}^e - \tilde{\boldsymbol{p}}_{eb}^e) \\ \mathbf{0}_{1\times3} & 1 & 0 \\ \mathbf{0}_{1\times3} & 0 & 1 \end{bmatrix} \\ &= \begin{bmatrix} \exp(\boldsymbol{\varphi}_l\times) & \mathrm{d}\boldsymbol{v} & \mathrm{d}\boldsymbol{p} \\ \mathbf{0}_{1\times3} & 1 & 0 \\ \mathbf{0}_{1\times3} & 0 & 1 \end{bmatrix}. \end{aligned} \tag{23}$$

Where $\tilde{C}_e^b$, $\tilde{\boldsymbol{v}}_{ib}^e$, and $\tilde{\boldsymbol{p}}_{eb}^e$ are the error-contaminated navigation parameters. The attitude error angle corresponding to $\tilde{C}_e^b C_b^e$ is the Euler angle $\boldsymbol{\varphi}_l$. If $\boldsymbol{\varphi}_l$ assumed to be a small value, $\tilde{C}_e^b C_b^e$ can be approximated as $\boldsymbol{I}_{3\times3} + \boldsymbol{\varphi}_l\times$. $\mathrm{d}\boldsymbol{v}$ and $\mathrm{d}\boldsymbol{p}$ are the velocity and position error vectors corresponding to (23) and can be derived as

$$\mathrm{d}\boldsymbol{v} = \tilde{C}_e^b(\boldsymbol{v}_{ib}^e - \tilde{\boldsymbol{v}}_{ib}^e) = -\tilde{C}_e^b\delta\boldsymbol{v}_{ib}^e \tag{24}$$

$$\mathrm{d}\boldsymbol{p} = \tilde{C}_e^b(\boldsymbol{p}_{eb}^e - \tilde{\boldsymbol{p}}_{eb}^e) = -\tilde{C}_e^b\delta\boldsymbol{p}_{eb}^e. \tag{25}$$

According to [33], the differential forms of $\boldsymbol{\varphi}_l$, $\mathrm{d}\boldsymbol{v}$, and $\mathrm{d}\boldsymbol{p}$ can be written as

$$\dot{\boldsymbol{\varphi}}_l = -\tilde{\boldsymbol{\omega}}_{ib}^b \times \boldsymbol{\varphi}_l - \delta\boldsymbol{\omega}_{ib}^b \tag{26}$$

$$\mathrm{d}\dot{\boldsymbol{v}} = -\tilde{\boldsymbol{\omega}}_{ib}^b \times \mathrm{d}\boldsymbol{v} - \delta\boldsymbol{f}^b - \tilde{\boldsymbol{f}}^b \times \boldsymbol{\varphi}_l \tag{27}$$

$$\mathrm{d}\dot{\boldsymbol{p}} = \mathrm{d}\boldsymbol{v} - \tilde{\boldsymbol{\omega}}_{ib}^b \times \mathrm{d}\boldsymbol{p} \tag{28}$$

where $\delta\boldsymbol{\omega}_{ib}^b$ and $\delta\boldsymbol{f}^b$ are the measurement errors of the gyroscope and accelerometer, respectively. Since the SINS used in this paper is a high-precision SINS and has been accurately calibrated, $\delta\boldsymbol{\omega}_{ib}^b$ and $\delta\boldsymbol{f}^b$ can be modeled as follows

$$\delta\boldsymbol{\omega}_{ib}^b = \boldsymbol{\varepsilon}_{ib}^b + \boldsymbol{\varepsilon}_w \tag{29}$$

$$\delta\boldsymbol{f}^b = \boldsymbol{\nabla}_{ib}^b + \boldsymbol{\nabla}_w \tag{30}$$

where $\boldsymbol{\varepsilon}_w$ and $\boldsymbol{\nabla}_w$ denote the noise of the gyroscope and accelerometer, respectively.

Based on (3), the velocity of the LDV in the *e* frame is given as follows

$$\begin{aligned} \boldsymbol{v}_{\text{LDV}}^e &= \tilde{C}_b^e C_m^b \boldsymbol{v}_{\text{LDV}}^m = C_b^e C_e^b \tilde{C}_b^e C_m^b \boldsymbol{v}_{\text{LDV}}^m \\ &\approx C_b^e(\boldsymbol{I}_3 - \boldsymbol{\varphi}_l\times)(\boldsymbol{I}_3 - \boldsymbol{\phi}_m\times)(1 + \delta K)\boldsymbol{v}^m. \end{aligned} \tag{31}$$

According to (26)–(31), the error state vector and state equation are given as

$$\boldsymbol{x} = \begin{bmatrix} \boldsymbol{\varphi}_l{}^T & \mathrm{d}\boldsymbol{v}^T & \mathrm{d}\boldsymbol{p}^T & \left(\boldsymbol{\varepsilon}_{ib}^b\right)^T & \left(\boldsymbol{\nabla}_{ib}^b\right)^T & \phi_{mx} & \phi_{mz} & \delta K \end{bmatrix}^T \tag{32}$$

$$\dot{\boldsymbol{x}} = \boldsymbol{F}\boldsymbol{x} + \boldsymbol{G}\boldsymbol{w} \tag{33}$$

$$\boldsymbol{F} = \begin{bmatrix} -\tilde{\boldsymbol{\omega}}_{ib}^b\times & \mathbf{0}_{3\times3} & \mathbf{0}_{3\times3} & -\boldsymbol{I}_3 & \mathbf{0}_{3\times3} & \mathbf{0}_{3\times3} \\ -\tilde{\boldsymbol{f}}^b\times & -\tilde{\boldsymbol{\omega}}_{ib}^b\times & \mathbf{0}_{3\times3} & \mathbf{0}_{3\times3} & -\boldsymbol{I}_3 & \mathbf{0}_{3\times3} \\ \mathbf{0}_{3\times3} & \boldsymbol{I}_3 & -\tilde{\boldsymbol{\omega}}_{ib}^b\times & \mathbf{0}_{3\times3} & \mathbf{0}_{3\times3} & \mathbf{0}_{3\times3} \\ \mathbf{0}_{9\times3} & \mathbf{0}_{9\times3} & \mathbf{0}_{9\times3} & \mathbf{0}_{9\times3} & \mathbf{0}_{9\times3} & \mathbf{0}_{9\times3} \end{bmatrix} \tag{34}$$

$$\boldsymbol{G} = \begin{bmatrix} -\boldsymbol{I}_3 & \mathbf{0}_{3\times3} \\ \mathbf{0}_{3\times3} & -\boldsymbol{I}_3 \\ \mathbf{0}_{12\times3} & \mathbf{0}_{12\times3} \end{bmatrix} \tag{35}$$

$$\boldsymbol{w} = \begin{bmatrix} \boldsymbol{\varepsilon}_w & \boldsymbol{\nabla}_w \end{bmatrix}^T. \tag{36}$$

Equation (34) shows that the state transition matrix is independent of the global state, even if the errors of the inertial sensor are taken into account. This indicates that the navigation errors will not affect the accuracy of the error differential equations. Therefore, the state equations can still accurately describe the error propagation law in the case of a large initial navigation error or when the system suffers from an outlier interference that causes a sudden increase in the navigation error.

3.3. Measurement model

In this subsection, two different measurement models are derived based on the Lie group $SE_2(3)$-based process model given in the previous subsection. First, the velocity measurement model is derived based on the projection of the velocity output of the LDV in the e-frame. Then, the velocity measurement model is extended to a displacement increment measurement model.

3.3.1. Velocity measurement model. The velocity measurement model is widely used for SINS/LDV and SINS/OD integration because both LDV and OD are velocity sensors. Performing error perturbation on v^e_{LDV} and ignoring the small higher-order error, the velocity error model of the LDV is given as

$$\delta \boldsymbol{v}^e_{\mathrm{LDV}} \approx \boldsymbol{C}^e_b (\boldsymbol{v}^m \times) \boldsymbol{\varphi}_l + \boldsymbol{C}^e_b (\boldsymbol{v}^m \times) \boldsymbol{\phi}_m + \boldsymbol{C}^e_b \boldsymbol{v}^m \delta K. \quad (37)$$

Based on (21), (22), (24), (25) and (37), and the conclusion from [33, 40] that 'Applying a linear function to the innovation term of an EKF before computing the gains does not change the results of the filter', the established measurement equation using the velocity measurement model is

$$\boldsymbol{z} = \begin{bmatrix} \tilde{\boldsymbol{C}}^b_e (\tilde{\boldsymbol{v}}^e_{ib} - \boldsymbol{z}_{\mathrm{GNSS},1}) \\ \tilde{\boldsymbol{C}}^b_e (\tilde{\boldsymbol{p}}^e_{eb} - \boldsymbol{z}_{\mathrm{GNSS},2}) \\ \boldsymbol{C}^b_e (\boldsymbol{v}^e_{\mathrm{LDV}} - \boldsymbol{v}^e_{\mathrm{GNSS}}) \end{bmatrix} = \boldsymbol{H}\boldsymbol{x} + \boldsymbol{v} \quad (38)$$

$$\boldsymbol{H} = \begin{bmatrix} \boldsymbol{0}_{6\times3} & -\boldsymbol{I}_6 & \boldsymbol{0}_{6\times6} & \boldsymbol{0}_{6\times2} & \boldsymbol{0}_{6\times1} \\ \boldsymbol{v}^m\times & \boldsymbol{0}_{3\times6} & \boldsymbol{0}_{3\times6} & \boldsymbol{C}_v & \boldsymbol{v}^m \end{bmatrix} \quad (39)$$

where $\boldsymbol{C}_v$ is the same as the one defined in (9).

3.3.2. Displacement incremental measurement model. The calibration method based on the velocity measurement model can calibrate the error term of the SINS/LDV integration very accurately when the vehicle is moving smoothly and the sensors are working normally during the calibration process. However, in reality, the vehicle may experience severe bumps and vibrations, which 1D-LDV cannot measure, and this causes additional deviation between the velocities of LDV and GNSS when the vehicle is vibrating. Moreover, the output values of LDV and GNSS may have different levels of error (noise and outliers) due to environmental factors in reality. Furthermore, LDV has a much higher output frequency than GNSS, which leads to data wastage from LDV when using the velocity measurement model. To minimize the impact of vehicle vibration and velocity noise on the calibration process and enhance the robustness of the calibration process and the data utilization efficiency of LDV, we extend the velocity measurement model to a displacement increment measurement model.

By integrating the velocity difference between the LDV and GNSS output velocities in the e frame, the following equation can be obtained:

$$\int_{\Delta t} \boldsymbol{v}^e_{\mathrm{LDV}} - \boldsymbol{v}^e_{\mathrm{GNSS}} \mathrm{d}t = \int_{\Delta t} \boldsymbol{C}^e_b (\boldsymbol{v}^m \times) \boldsymbol{\varphi}_l \mathrm{d}t$$
$$+ \int_{\Delta t} \boldsymbol{C}^e_b (\boldsymbol{v}^m \times) \boldsymbol{\phi}_m \mathrm{d}t + \int_{\Delta t} \boldsymbol{C}^e_b \boldsymbol{v}^m \delta K \mathrm{d}t \quad (40)$$

where Δt is the time interval for integration, and in this paper, it was set as 1 s. Considering that the IMU used in this paper is a high-precision IMU and Δt is small, the SINS misalignment angle error $\boldsymbol{\varphi}_l$ can be regarded as a constant value. Suppose that there are M epochs during the integration time, (40) can be rewritten as:

$$\int_{\Delta t} \boldsymbol{v}^e_{\mathrm{LDV}} - \boldsymbol{v}^e_{\mathrm{GNSS}} \mathrm{d}t = \sum_{k=s-M}^{s-1} \int_{t_k}^{t_{k+1}} \boldsymbol{C}^{e(t)}_{b(t)} \left(\boldsymbol{v}^m_{(t)} \times \right) \boldsymbol{\varphi}_l \mathrm{d}t$$
$$+ \sum_{k=s-M}^{s-1} \int_{t_k}^{t_{k+1}} \boldsymbol{C}^{e(t)}_{b(t)} \left(\boldsymbol{v}^m_{(t)} \times \right) \boldsymbol{\phi}_m \mathrm{d}t$$
$$+ \sum_{k=s-M}^{s-1} \int_{t_k}^{t_{k+1}} \boldsymbol{C}^{e(t)}_{b(t)} \boldsymbol{v}^m_{(t)} \delta K \mathrm{d}t \quad (41)$$

where

$$\boldsymbol{C}^{e(t)}_{b(t)} = \boldsymbol{C}^{e(t)}_{e(t_k)} \boldsymbol{C}^{e(t_k)}_{b(t_k)} \boldsymbol{C}^{b(t_k)}_{b(t)} \quad (42)$$

$$\boldsymbol{C}^{e(t)}_{e(t_k)} \approx \boldsymbol{I}_3 - \boldsymbol{\varphi}_e \times = \boldsymbol{I}_3 - ((t - t_k)\boldsymbol{\omega}^e_{ie}) \times \quad (43)$$

$$\boldsymbol{C}^{b(t_k)}_{b(t)} \approx \boldsymbol{I}_3 + \left(\int_{t_k}^t \boldsymbol{\omega}^b_{ib} \mathrm{d}\tau \right) \times . \quad (44)$$

By approximating the incremental integral in (44) using the two-sample correction, and assuming that the velocity $\boldsymbol{v}^m$ changes linearly during Δt, $\int_{t_k}^{t_{k+1}} \boldsymbol{C}^{e(t)}_{b(t)}(\boldsymbol{v}^m_{(t)} \times)\boldsymbol{\varphi}_l dt$ can be further written as:

$$\int_{t_k}^{t_{k+1}} \boldsymbol{C}^{e(t)}_{b(t)} \left(\boldsymbol{v}^m_{(t)} \times \right) \boldsymbol{\varphi}_l \mathrm{d}t$$
$$= \int_{t_k}^{t_{k+1}} \boldsymbol{C}^{e(t)}_{e(t_k)} \boldsymbol{C}^{e(t_k)}_{b(t_k)} \boldsymbol{C}^{b(t_k)}_{b(t)} \left(\boldsymbol{v}^m_{(t_k)} + \frac{t - t_k}{T} \left(\boldsymbol{v}^m_{(t_{k+1})} - \boldsymbol{v}^m_{(t_k)} \right) \right) \times \boldsymbol{\varphi}_l \mathrm{d}t$$
$$= \left\{ T \boldsymbol{C}^{e(t_k)}_{b(t_k)} \left(\left(\frac{\boldsymbol{v}^m_{(t_k)} + \boldsymbol{v}^m_{(t_{k+1})}}{2} \right) \times \right) - \frac{T^2}{6} (\boldsymbol{\omega}^e_{ie} \times) \boldsymbol{C}^{e(t_k)}_{b(t_k)} \left(\boldsymbol{v}^m_{(t_k)} \times \right) \right.$$
$$- \frac{T^2}{3} \boldsymbol{\omega}^e_{ie} \times \boldsymbol{C}^{e(t_k)}_{b(t_k)} \left(\boldsymbol{v}^m_{(t_{k+1})} \times \right) + \frac{T}{3} \boldsymbol{C}^{e(t_k)}_{b(t_k)} (\Delta \boldsymbol{\theta}_1 \times) \left(\boldsymbol{v}^m_{(t_k)} \times \right)$$
$$+ \frac{T}{6} \boldsymbol{C}^{e(t_k)}_{b(t_k)} ((3\Delta \boldsymbol{\theta}_1 + \Delta \boldsymbol{\theta}_2) \times) \left(\boldsymbol{v}^m_{(t_{k+1})} \times \right)$$
$$- \frac{T^2}{20} (\boldsymbol{\omega}^e_{ie} \times) \boldsymbol{C}^{e(t_k)}_{b(t_k)} ((7\Delta \boldsymbol{\theta}_1 + 3\Delta \boldsymbol{\theta}_2) \times) \left(\boldsymbol{v}^m_{(t_{k+1})} \times \right)$$
$$\left. - \frac{T^2}{60} (\boldsymbol{\omega}^e_{ie} \times) \boldsymbol{C}^{e(t_k)}_{b(t_k)} ((9\Delta \boldsymbol{\theta}_1 + \Delta \boldsymbol{\theta}_2) \times) \left(\boldsymbol{v}^m_{(t_k)} \times \right) \right\} \boldsymbol{\varphi}_l \quad (45)$$

where T is the sampling interval of the SINS and LDV, and $\Delta t = MT$.

The discretization of $\int_{t_k}^{t_{k+1}} \boldsymbol{C}^{e(t)}_{b(t)}(\boldsymbol{v}^m_{(t)} \times)\boldsymbol{\phi}_m \mathrm{d}t$ and $\int_{t_k}^{t_{k+1}} \boldsymbol{C}^{e(t)}_{b(t)} \boldsymbol{v}^m_{(t)} \delta K \mathrm{d}t$ is similar to (45).

According to (41), the established measurement equation based on the displacement increment measurement model is

$$z = \begin{bmatrix} \tilde{C}_e^b (\tilde{v}_{ib}^e - z_{\text{GNSS},1}) \\ \tilde{C}_e^b (\tilde{p}_{eb}^e - z_{\text{GNSS},2}) \\ \int_{\Delta t} v_{\text{LDV}}^e - v_{\text{GNSS}}^e \, \mathrm{d}t \end{bmatrix} = Hx + v \qquad (46)$$

where H can be obtained according to (39) and (41).

3.4. Initial covariance setting

Unlike the error states in the traditional SINS/LDV calibration method, which assumes that each error state is mutually independent, the error states shown in (24) and (25) are coupled with each other. Therefore, according to (17), (24) and (25), the initial covariance matrix can be set to the following form in the Lie group $SE_2(3)$-based SINS/LDV online calibration method:

$$P_{l,0}^e = T_l P_0^e T_l^T \qquad (47)$$

$$T_l = \begin{bmatrix} T_{avp,l} & \mathbf{0}_{3\times3} & \mathbf{0}_{3\times3} & \mathbf{0}_{3\times3} \\ \mathbf{0}_{3\times9} & I_3 & \mathbf{0}_{3\times3} & \mathbf{0}_{3\times3} \\ \mathbf{0}_{3\times9} & \mathbf{0}_{3\times3} & I_3 & \mathbf{0}_{3\times3} \\ \mathbf{0}_{3\times9} & \mathbf{0}_{3\times3} & \mathbf{0}_{3\times3} & I_3 \end{bmatrix} \qquad (48)$$

$$T_{avp,l} = \begin{bmatrix} I_3 & \mathbf{0}_{3\times3} & \mathbf{0}_{3\times3} \\ \mathbf{0}_{3\times3} & -C_{e,0}^b & -C_{e,0}^b (\omega_{ie}^e \times) \\ \mathbf{0}_{3\times3} & \mathbf{0}_{3\times3} & -C_{e,0}^b \end{bmatrix}. \qquad (49)$$

3.5. Feedback correction

Feedback correction of the navigation parameters is necessary after estimating the error state. The feedback correction at time k for the Lie group $SE_2(3)$-based SINS/LDV online calibration method can be expressed as:

$$C_{b,k}^e = \tilde{C}_{b,k}^e \exp(\varphi_{l,k}) \qquad (50)$$

$$v_{ib,k}^e = \tilde{v}_{ib,k}^e + \tilde{C}_{b,k}^e \mathrm{d}v_k \qquad (51)$$

$$p_{eb,k}^e = \tilde{p}_{eb,k}^e + \tilde{C}_{b,k}^e \mathrm{d}p_k. \qquad (52)$$

After the feedback correction, the corresponding error state estimate should be reset to zero, that is, $x(1:9) = \mathbf{0}_{9\times1}$, and the system goes to the next filtering cycle.

4. The SINS/ LDV calibration model based on Lie group $SE_3(3)$

For the SINS/LDV calibration system based on $SE_2(3)$, the displacement incremental measurement model is proposed to enhance the robustness of the calibration process and the data utilization of the LDV. However, as shown in (41) and (45), after integrating and discretizing the velocity measurements, it is not suitable to multiply by an attitude matrix in the observations as in (38) and thus make the measurement transition matrix attitude-independent. Therefore, its measurement transition matrix based on the displacement incremental measurement model is attitude-dependent, and the displacement incremental measurement model is more sensitive to large misalignment angles than the velocity measurement model. To achieve high robustness and data utilization efficiency as well as attitude-independent process and measurement models for the calibration system, a Lie group $SE_3(3)$ and GNSS-based online calibration method for SINS/LDV integrated navigation system is proposed in this section. In this method, the left-invariant observation-SINS/LDV DR position is formulated as elements of the Lie group $SE_3(3)$ together with the attitude, velocity, and position calculated by SINS in the process model of the calibration system.

4.1. Process model

The DR position of the SINS/LDV integration has the following relationship to the LDV measurements:

$$\dot{p}_{eb,\text{DR}}^e = v_{\text{LDV}}^e. \qquad (53)$$

Given an initial position and using the LDV velocity in e frame derived from (31), DR can be performed. Assuming that other influencing factors are negligible, the error $\delta p_{eb,\text{DR}}^e$ between the DR-estimated position $\tilde{p}_{eb,\text{DR}}^e$ and the true position p_{eb}^e can be considered to be caused by the error in (31). That is, the δK and the ϕ_m eventually affect the position accuracy of the integrated navigation system.

Similar to the (19), the C_b^e, v_{ib}^e, p_{eb}^e, and $p_{eb,\text{DR}}^e$ can be embedded as the element χ of the group $SE_3(3)$

$$\chi = \begin{bmatrix} C_b^e & v_{ib}^e & p_{eb}^e & p_{eb,\text{DR}}^e \\ \mathbf{0}_{1\times3} & 1 & 0 & 0 \\ \mathbf{0}_{1\times3} & 0 & 1 & 0 \\ \mathbf{0}_{1\times3} & 0 & 0 & 1 \end{bmatrix}. \qquad (54)$$

Similar to p_{GNSS}^e, $p_{eb,\text{DR}}^e$ is also a type of left-invariant measurement, so the left-invariant group error is used

$$
\begin{aligned}
\boldsymbol{\eta} &= \tilde{\boldsymbol{\chi}}^{-1} \boldsymbol{\chi} \\
&= \begin{bmatrix}
\tilde{\boldsymbol{C}}_e^b \boldsymbol{C}_b^e & \tilde{\boldsymbol{C}}_e^b \left(\boldsymbol{v}_{ib}^e - \tilde{\boldsymbol{v}}_{ib}^e \right) & \tilde{\boldsymbol{C}}_e^b \left(\boldsymbol{p}_{eb}^e - \tilde{\boldsymbol{p}}_{eb}^e \right) & \tilde{\boldsymbol{C}}_e^b \left(\boldsymbol{p}_{eb,\mathrm{DR}}^e - \tilde{\boldsymbol{p}}_{eb,\mathrm{DR}}^e \right) \\
\boldsymbol{0}_{1\times3} & 1 & 0 & 0 \\
\boldsymbol{0}_{1\times3} & 0 & 1 & 0 \\
\boldsymbol{0}_{1\times3} & 0 & 0 & 1
\end{bmatrix} \\
&= \begin{bmatrix}
\exp\left(\boldsymbol{\varphi}_l \times \right) & \mathrm{d}\boldsymbol{v} & \mathrm{d}\boldsymbol{p} & \mathrm{d}\boldsymbol{p}_{\mathrm{DR}} \\
\boldsymbol{0}_{1\times3} & 1 & 0 & 0 \\
\boldsymbol{0}_{1\times3} & 0 & 1 & 0 \\
\boldsymbol{0}_{1\times3} & 0 & 0 & 1
\end{bmatrix}
\end{aligned}
\tag{55}
$$

where $\tilde{\boldsymbol{p}}_{eb,\mathrm{DR}}^e$ is the DR position of SINS/LDV integration with error contamination. $\mathrm{d}\boldsymbol{p}_{\mathrm{DR}}$ is the DR position error vector corresponding to (50) and can be derived as

$$
\mathrm{d}\boldsymbol{p}_{\mathrm{DR}} = \tilde{\boldsymbol{C}}_e^b \left(\boldsymbol{p}_{eb,\mathrm{DR}}^e - \tilde{\boldsymbol{p}}_{eb,\mathrm{DR}}^e \right) = -\tilde{\boldsymbol{C}}_e^b \delta \boldsymbol{p}_{eb,\mathrm{DR}}^e.
\tag{56}
$$

According to (17) and (53), the error model of $\mathrm{d}\boldsymbol{p}_{\mathrm{DR}}$ can be easily derived as follows:

$$
\begin{aligned}
\mathrm{d}\dot{\boldsymbol{p}}_{\mathrm{DR}} &= \dot{\tilde{\boldsymbol{C}}}_e^b \left(\boldsymbol{p}_{eb,\mathrm{DR}}^e - \tilde{\boldsymbol{p}}_{eb,\mathrm{DR}}^e \right) + \tilde{\boldsymbol{C}}_e^b \left(\dot{\boldsymbol{p}}_{eb,\mathrm{DR}}^e - \dot{\tilde{\boldsymbol{p}}}_{eb,\mathrm{DR}}^e \right) \\
&= -\left(\tilde{\boldsymbol{C}}_e^b \left(\tilde{\boldsymbol{\omega}}_{ie}^e \times \right) - \left(\tilde{\boldsymbol{\omega}}_{ib}^b \times \right) \tilde{\boldsymbol{C}}_e^b \right) \delta \boldsymbol{p}_{eb,\mathrm{DR}}^e + \tilde{\boldsymbol{C}}_e^b \left(\boldsymbol{v}^e - \boldsymbol{v}_{\mathrm{LDV}}^e \right)
\end{aligned}
$$

$$
\begin{aligned}
&= -\left(\tilde{\boldsymbol{\omega}}_{ib}^b \times \right) \mathrm{d}\boldsymbol{p}_{\mathrm{DR}} - \tilde{\boldsymbol{C}}_e^b \left(\tilde{\boldsymbol{\omega}}_{ie}^e \times \right) \tilde{\boldsymbol{C}}_b^e \tilde{\boldsymbol{C}}_e^b \delta \boldsymbol{p}_{eb,\mathrm{DR}}^e \\
&\quad + \tilde{\boldsymbol{C}}_e^b \left(\boldsymbol{v}^e - \boldsymbol{v}_{\mathrm{LDV}}^e \right) \\
&\approx -\left(\tilde{\boldsymbol{\omega}}_{ib}^b \times \right) \mathrm{d}\boldsymbol{p}_{\mathrm{DR}} + \left(\tilde{\boldsymbol{\omega}}_{ie}^b \times \right) \mathrm{d}\boldsymbol{p}_{\mathrm{DR}} \\
&\quad + \tilde{\boldsymbol{C}}_e^b \left(-\boldsymbol{C}_b^e \left(\boldsymbol{v}^m \times \right) \boldsymbol{\varphi}_l - \boldsymbol{C}_b^e \left(\boldsymbol{v}^m \times \right) \boldsymbol{\phi}_m - \boldsymbol{C}_b^e \boldsymbol{v}^m \delta K \right) \\
&\approx -\left(\boldsymbol{\omega}_{eb}^b \times \right) \mathrm{d}\boldsymbol{p}_{\mathrm{DR}} - \left(\boldsymbol{v}^m \times \right) \boldsymbol{\varphi}_l - \left(\boldsymbol{v}^m \times \right) \boldsymbol{\phi}_m - \boldsymbol{v}^m \delta K.
\end{aligned}
\tag{57}
$$

According to (26)–(30) and (57), the error state vector is defined as follows:

$$
\boldsymbol{x} = \begin{bmatrix} \boldsymbol{\varphi}_l^T & \mathrm{d}\boldsymbol{v}^T & \mathrm{d}\boldsymbol{p}^T & \mathrm{d}\boldsymbol{p}_{\mathrm{DR}}^T & \left(\boldsymbol{\varepsilon}_{ib}^b \right)^T & \left(\boldsymbol{\nabla}_{ib}^b \right)^T & \phi_{mx} & \phi_{mz} & \delta K \end{bmatrix}^T.
\tag{58}
$$

Based on (26)–(28) and (57), the state transition matrix $\boldsymbol{F}$ and noise transfer matrix $\boldsymbol{G}$ can be expressed as:

$$
\boldsymbol{F} = \begin{bmatrix}
-\tilde{\boldsymbol{\omega}}_{ib}^b \times & \boldsymbol{0}_{3\times3} & \boldsymbol{0}_{3\times3} & \boldsymbol{0}_{3\times3} & -\boldsymbol{I}_3 & \boldsymbol{0}_{3\times3} & \boldsymbol{0}_{3\times2} & \boldsymbol{0} \\
-\tilde{\boldsymbol{f}}^b \times & -\tilde{\boldsymbol{\omega}}_{ib}^b \times & \boldsymbol{0}_{3\times3} & \boldsymbol{0}_{3\times3} & \boldsymbol{0}_{3\times3} & -\boldsymbol{I}_3 & \boldsymbol{0}_{3\times2} & \boldsymbol{0} \\
\boldsymbol{0}_{3\times3} & \boldsymbol{I}_3 & -\tilde{\boldsymbol{\omega}}_{ib}^b \times & \boldsymbol{0}_{3\times3} & \boldsymbol{0}_{3\times3} & \boldsymbol{0}_{3\times3} & \boldsymbol{0}_{3\times2} & \boldsymbol{0} \\
-\boldsymbol{v}^m \times & \boldsymbol{0}_{3\times3} & \boldsymbol{0}_{3\times3} & -\boldsymbol{\omega}_{eb}^b \times & \boldsymbol{0}_{3\times3} & \boldsymbol{0}_{3\times3} & \boldsymbol{C}_v & \boldsymbol{v}^m \\
\boldsymbol{0}_{9\times3} & \boldsymbol{0}_{9\times3} & \boldsymbol{0}_{9\times3} & \boldsymbol{0}_{9\times3} & \boldsymbol{0}_{9\times3} & \boldsymbol{0}_{9\times3} & \boldsymbol{0}_{9\times2} & \boldsymbol{0}_{9\times1}
\end{bmatrix}
\tag{59}
$$

$$
\boldsymbol{G} = \begin{bmatrix}
-\boldsymbol{I}_3 & \boldsymbol{0}_{3\times3} \\
\boldsymbol{0}_{3\times3} & -\boldsymbol{I}_3 \\
\boldsymbol{0}_{15\times3} & \boldsymbol{0}_{15\times3}
\end{bmatrix}.
\tag{60}
$$

Even though the differential equation for the left-invariant error $\boldsymbol{\eta}$ is not trajectory-independent due to the presence of $\boldsymbol{\omega}_{eb}^b$ ($\boldsymbol{\omega}_{eb}^b = \boldsymbol{\omega}_{ib}^b - \boldsymbol{C}_e^b \boldsymbol{\omega}_{ie}^e$), $\boldsymbol{\omega}_{ie}^e$ is much smaller than $\boldsymbol{\omega}_{ib}^b$ during vehicle motion, so that $\boldsymbol{\omega}_{eb}^b$ can be approximated as $\boldsymbol{\omega}_{ib}^b$, and thus the state transition matrix can be considered independent of the global state.

4.2. Measurement model

Similar to (38), the transformed measurement equation is established as

$$z = \begin{bmatrix} \tilde{C}_e^b \left(\tilde{v}_{ib}^e - z_{\mathrm{GNSS},1} \right) \\ \tilde{C}_e^b \left(\tilde{p}_{eb}^e - z_{\mathrm{GNSS},2} \right) \\ \tilde{C}_e^b \left(\tilde{p}_{eb,\mathrm{DR}}^e - z_{\mathrm{GNSS},2} \right) \end{bmatrix} = Hx + v \qquad (61)$$

$$H = \begin{bmatrix} \mathbf{0}_{6\times3} & -I_6 & \mathbf{0}_{6\times3} & \mathbf{0}_{6\times9} \\ \mathbf{0}_{3\times3} & \mathbf{0}_{3\times6} & -I_3 & \mathbf{0}_{3\times9} \end{bmatrix}. \qquad (62)$$

As shown in (62), the measurement transition matrix H is independent of the trajectory, and by utilizing the attitude error-immune process model (59) and the trajectory-independent measurement model (62), the Lie group $SE_3(3)$-based online calibration method for SINS/LDV proposed in this section can achieve the initial alignment as well as the online calibration of the system even with large initial attitude errors.

4.3. Initial covariance setting and error feedback correction

Based on (48) and (56), the initial covariance transition matrix T_l is set as follows in the Lie group $SE_2(3)$-based SINS/LDV online calibration method:

$$T_l = \begin{bmatrix} T_{avp,l} & \mathbf{0}_{3\times3} & \mathbf{0}_{3\times3} & \mathbf{0}_{3\times3} & \mathbf{0}_{3\times3} \\ \mathbf{0}_{3\times9} & -C_{e,0}^b & \mathbf{0}_{3\times3} & \mathbf{0}_{3\times3} & \mathbf{0}_{3\times3} \\ \mathbf{0}_{3\times9} & \mathbf{0}_{3\times3} & I_3 & \mathbf{0}_{3\times3} & \mathbf{0}_{3\times3} \\ \mathbf{0}_{3\times9} & \mathbf{0}_{3\times3} & \mathbf{0}_{3\times3} & I_3 & \mathbf{0}_{3\times3} \\ \mathbf{0}_{3\times9} & \mathbf{0}_{3\times3} & \mathbf{0}_{3\times3} & \mathbf{0}_{3\times3} & I_3 \end{bmatrix}. \qquad (63)$$

For the Lie group $SE_3(3)$-based SINS/LDV online calibration method proposed in this section, the feedback correction process includes feedback correction for SINS/LDV integrated DR position error in addition to (50)–(52). Similar to (52), the feedback correction at time k for the SINS/LDV integrated DR position error can be expressed as:

$$p_{eb,\mathrm{DR},k}^e = \tilde{p}_{eb,\mathrm{DR},k}^e + \tilde{C}_{b,k}^e \mathrm{d}p_{\mathrm{DR},k}. \qquad (64)$$

5. Vehicle-mounted field test

To evaluate the effectiveness and practical value of the calibration method proposed in this paper, we conducted two groups of vehicle-mounted tests. Figure 3 displays the test equipment, which includes a self-developed high-precision IMU, a self-made 1D-LDV, and a dual-antenna GNSS receiver. The high-precision IMU consists of three ring laser gyros and three quartz accelerometers with an output frequency of 100 Hz. The bias instability of the gyros is within 0.007°/h and their random walk is within 0.001°/√h. The bias instability of the accelerometers is within 50 μg and their random walk is 50 μg/√h. The velocity measurement error of the LDV is within 0.08% (1σ) with an output frequency of 100 Hz. The dual-antenna GNSS receiver integrates microelectromechanical system (MEMS) inertial sensors. The DGNSS receiver's

Figure 3. Installation diagram of the experimental system.

horizontal positioning accuracy, altitude positioning accuracy, and velocity accuracy are within 0.05 m, 0.05 m, and 0.03 m s^{-1}, respectively, with an output frequency of 10 Hz.

Two groups of field tests were conducted in Changsha City to evaluate our proposed calibration method. Before moving, the vehicle remained stationary for approximately 13 min at the initial location, where static attitude alignment was performed to obtain an accurate initial attitude. The outputs of dual-antenna differential GNSS were used to calibrate the SINS/LDV integrated navigation system. The reference position of the vehicle was determined by a high-precision SINS/GNSS integrated navigation system that combined a high-precision IMU and a dual-antenna differential GNSS, and applied the Rauch–Tung–Striebel smoothing algorithm to process the data.

To evaluate the performance of the proposed methods, we compare them with the most widely used calibration method based on a conventional Kalman filter. We denote the calibration method presented in section 2 as SO-KF, the calibration method based on the left error model (34) and the velocity measurement model (38) in section 3 as LSE-V-KF, the calibration method based on the left error model (34) and the displacement increment measurement model (46) in section 3 as LSE-DI-KF, and the calibration method based on the left error model (59) in section 4 as LSE-DR-KF.

The first vehicle experiment lasted for 2.08 h and the vehicle traveled a distance of 151.9 km. Figure 4 shows the trajectory of the vehicle and the output of the LDV during the experiment. Figures 5–7 show the calibration results of different methods in the first experiment. It can be seen that all the methods are able to estimate the error parameters of the SINS/LDV integrated navigation system, and the calibration results obtained by the four calibration methods are very close numerically. However, the calibration curves of the four calibration methods are subjected to different degrees of fluctuation during the calibration process, due to the effects of vehicle side-slip and other impacts brought about by the violent maneuvers of vehicles, as well as the poor GNSS
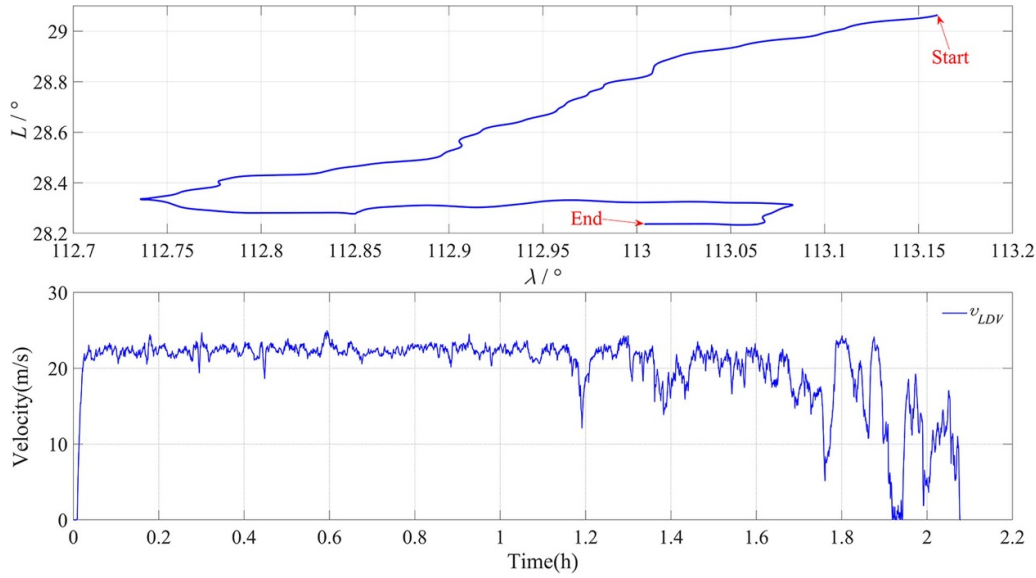
Figure 4. Trajectory of the vehicle and velocity curve of the LDV output in the first field test.
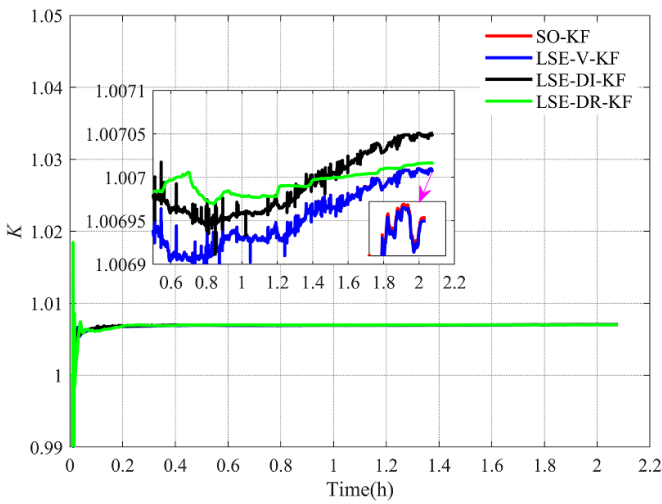
**Figure 5.** Curve of the scale factor in the first vehicle test.
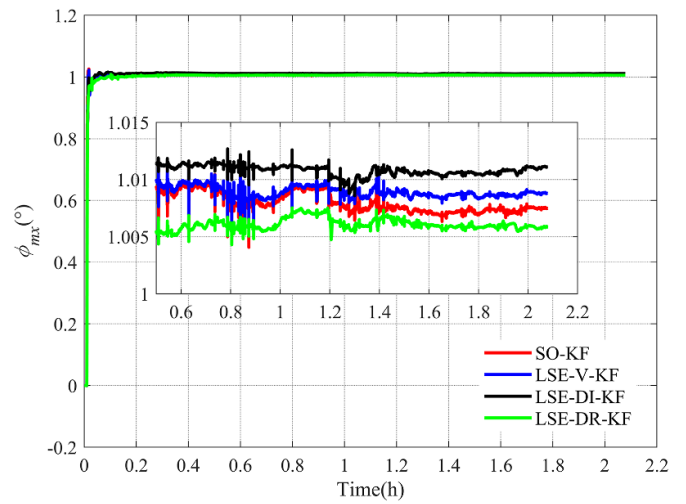
**Figure 6.** Curve of the pitch misalignment angle in the first vehicle test.

signals caused by a large number of flyovers and billboards on the highway. In terms of the fluctuation of the calibration curves, the LSE-DI-KF and LSE-DR-KF are less subjected to fluctuations than the SO-KF and LSE-V-KF, which is expected since displacement increment and DR position are known to be more stable and robust observables compared to velocity. Moreover, for LSE-V-KF and SO-KF, which also use velocity as an observation quantity, the calibration curve of LSE-V-KF is undoubtedly smoother than that of SO-KF, which is one of the benefits of applying the Lie group theory to the calibration of the combined navigation system. The global state-independent state transition matrix and the attitude-independent measurement transition matrix make the LSE-V-KF more advantageous than SO-KF in harsh environments. For both LSE-DI-KF and LSE-DR-KF, it is also reasonable that LSE-DR-KF performs smoother because noise and outliers have less effect on the DR position than displacement

increments, and because the measurement transition matrices of LSE-DR-KF are attitude-independent while those of LSE-DI-KF are attitude-dependent.

To evaluate the accuracy of the four calibration methods, the DR of the SINS/LDV integrated navigation system is performed using the calibration results, as the calibration accuracy of the SINS/LDV system is directly reflected in the positional error of the DR The smaller positional error indicates the higher calibration accuracy of the SINS/LDV system. Figure 8 compares the horizontal positioning error and ratio with respect to the distance travelled of different methods in the first test. Figure 9 shows the height positioning error of different methods in the first test. Table 1 summarizes the maximum (*Max*) and mean (*Mean*) position errors of the SINS/LDV integrated navigation system calibrated by four different methods in the first test.
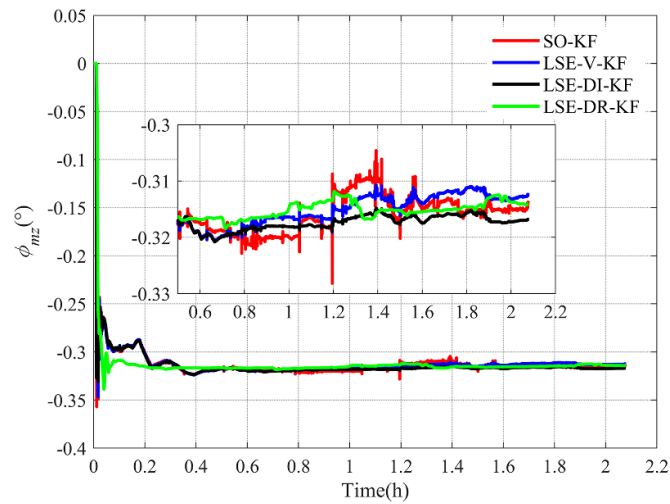
Figure 7. Curve of the heading misalignment angle in the first vehicle test.
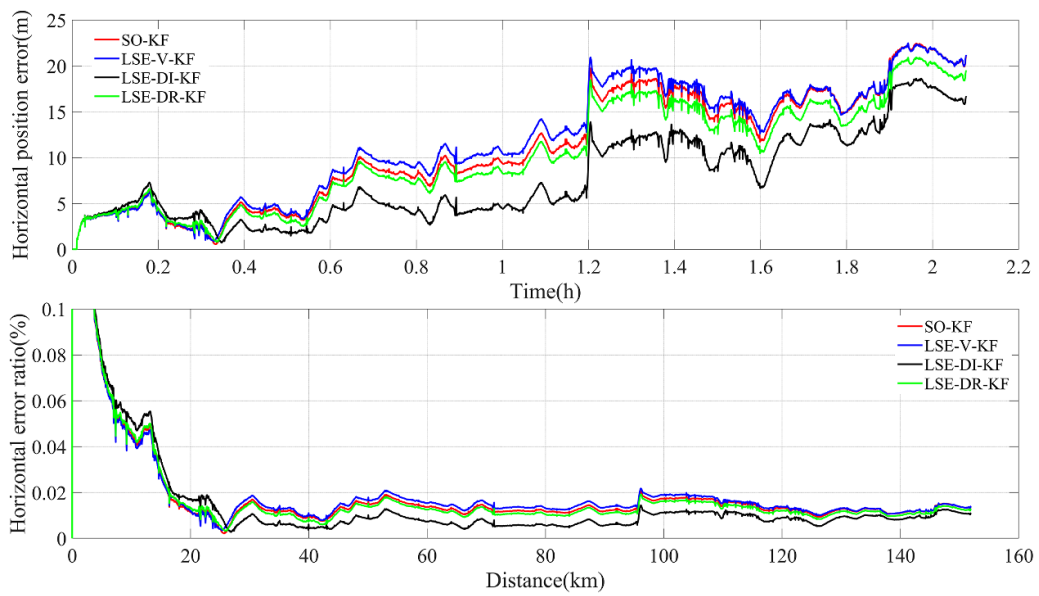
Figure 8. First test's horizontal location error and horizontal error ratio.
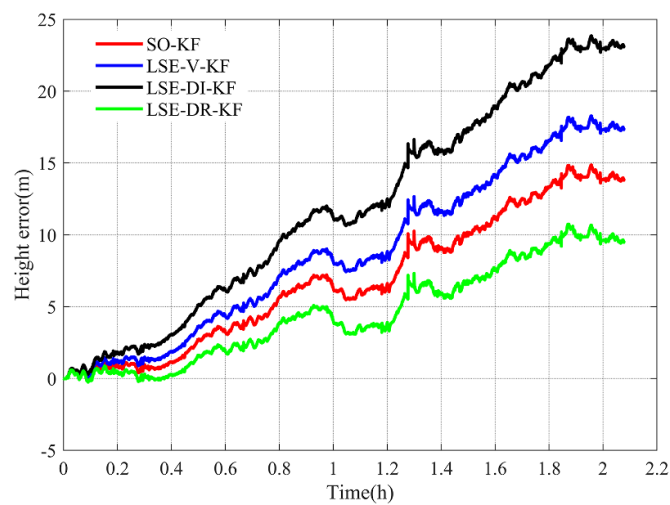
Figure 9. First test's height positioning error.

Table 1. Performance comparison of the four methods in the first test (151.9 km).

Methods		*Mean* (m)	Error ratio (‰)	*Max* (m)	Error ratio (‰)
SO-KF	Horizontal error	11.15	0.073	22.44	0.147
	Height error	6.83	0.045	14.86	0.098
LSE-V-KF	Horizontal error	11.77	0.077	22.48	0.148
	Height error	8.72	0.057	18.28	0.120
LSE-DI-KF	Horizontal error	7.75	0.051	18.61	0.123
	Height error	11.80	0.078	23.85	0.157
LSE-DR-KF	Horizontal error	10.30	0.068	20.92	0.137
	Height error	4.53	0.030	10.74	0.071

As shown in figures 8, 9 and table 1, the positioning accuracy of the SINS/LDV integrated navigation system varies with different calibration methods, but there is no significant difference in the calibration accuracy among the four calibration methods, which are generally at the same level. They are all able to calibrate the SINS/LDV integrated navigation system accurately, and keep the horizontal position error of SINS/LDV integrated navigation system within 0.02% of the mileage. Although the DR horizontal position errors of the SINS/LDV integrated navigation system calibrated by various methods are not much different from each other, there are still some differences among the methods. The errors of LSE-DI-KF and LSE-DR-KF are smaller than those of LSE-V-KF and SO-KF, indicating that using the displacement increment and the DR position as the filter observations is helpful to improve the calibration accuracy. The error of LSE-V-KF is slightly larger than that of SO-KF, indicating that LSE-V-KF is not necessarily better than SO-KF in normal experimental scenarios. Regarding the height error of DR, the four methods are not very accurate in estimating the pitch installation misalignment angle, but this is expected, because one-dimensional LDV (1D-LDV) cannot measure the vertical velocity of the vehicle, and the three-dimensional velocity of the vehicle obtained through LDV is based on the NHC assumption, that is, the vehicle has zero lateral and vertical velocity. However, strictly speaking, the vertical zero-velocity constraint in the NHC should be perpendicular to the ground rather than along the *Z*-axis in the *m* frame. Therefore, the pitch installation misalignment angle calibrated is actually the pitch misalignment angle between the IMU and the roadway rather than the pitch installation misalignment angle between the IMU and the LDV. Thus, for the integrated navigation system composed of the IMU and the 1D-LDV, factors such as vehicle maneuvering, vehicle load changes, vehicle tire status, and road surface conditions will affect the estimation of the pitch misalignment angle. According to [17], we give figure 10 to show the vertical velocity of the vehicle in the *m* frame during the first experiment. It can be seen that during the experiment, the vertical velocity of the vehicle in the *m* frame, although fluctuating above and below zero, does not satisfy the NHC assumption most of the time, which will affect the estimation of the pitch misalignment angle. Therefore, for the SINS/OD integrated navigation system and
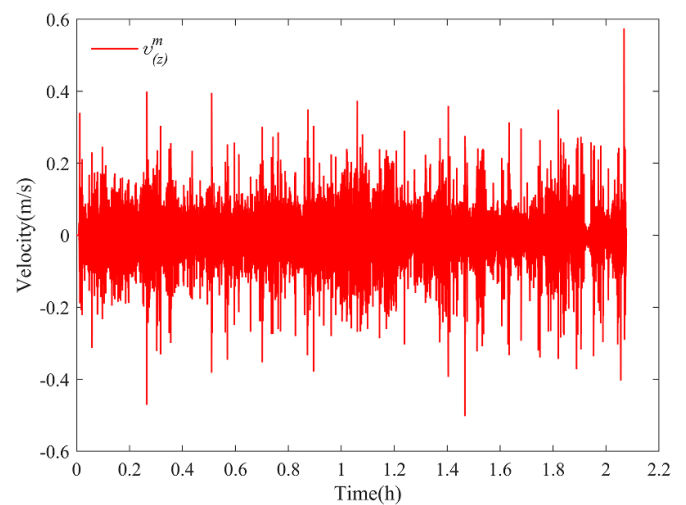
Figure 10. The vertical velocity of the vehicle in the *m* frame in the first test.

the SINS/1D-LDV integrated navigation system, people are more concerned about their horizontal positioning accuracy, and they also often use an atmospheric pressure altimeter to constrain the altitude information.

In section 3, we pointed out that the calibration method based on Lie group will show better performance than the calibration method based on traditional model when facing large misalignment angles. Therefore, we calibrate the SINS/LDV integrated navigation system without static attitude initial alignment based on the data from the first experiment. Figure 11 shows the attitude error results of the different methods during the calibration process. Figure 12 shows the calibration results of the different methods. Figure 13 shows the DR position error obtained from the calibration results in figure 12. As shown in figure 11, the attitude errors of LSE-V-KF and LSE-DR-KF converge significantly faster than those of LSE-DI-KF and SO-KF. They can both quickly converge the heading error to within 0.1° with an initial heading angle error of 159° for the integrated navigation system. Although the attitude errors of LSE-DI-KF converge less quickly than those of LSE-V-KF and LSE-DR-KF, they are better than SO-KF. Based on the results in figure 11, we can easily foresee that
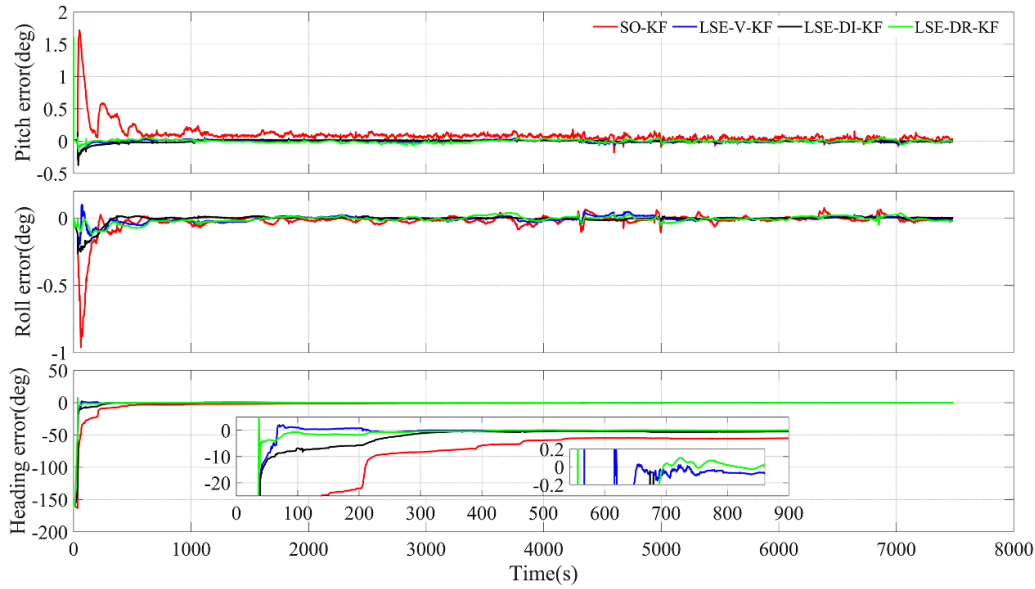
Figure 11. Attitude errors in the first large misalignment test.
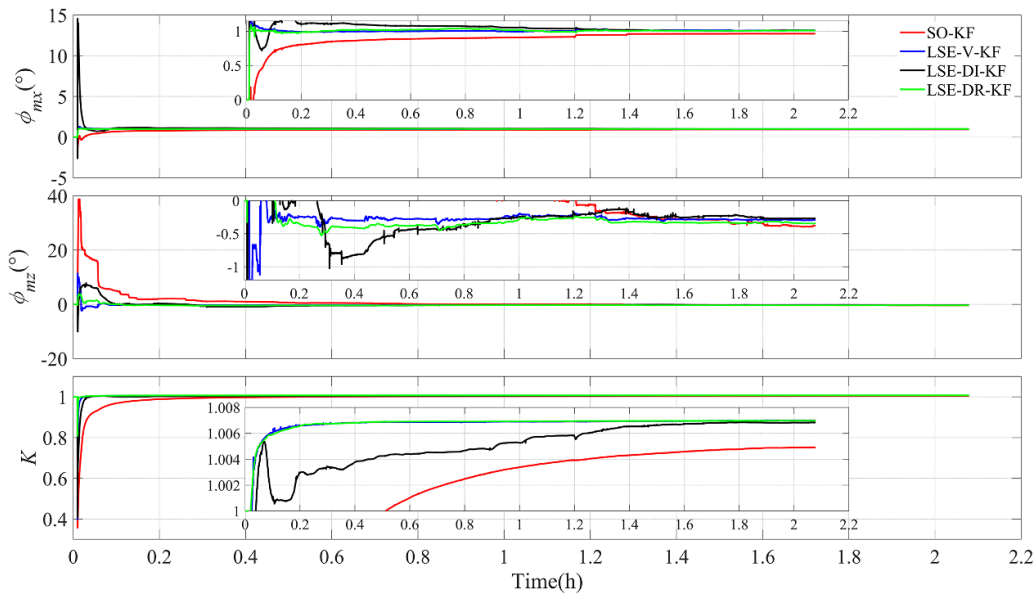

Figure 12. Calibration results in the first large misalignment test.

the calibration results of LSE-V-KF and LSE-DR-KF are better than those of LSE-DI-KF and SO-KF at large misalignment angles, because (9) and (46) show that the measurement transition matrices of LSE-DI-KF and SO-KF are attitude-dependent and when the attitude is no longer accurate, the calibration results of LSE-DI-KF and SO-KF will be affected. It is also obvious that the calibration results of LSE-DI-KF are better than those of SO-KF under large misalignment angle conditions because the process model of LSE-DI-KF is independent of the global state, unlike SO-KF. The calibration results in figure 12 and the DR position errors in figure 13 are consistent with the analysis performed based on figure 11.

To further verify the effectiveness and evaluate the accuracy of the proposed calibration method, a second vehicle test

was conducted that lasted 1.67 h and covered a total distance of 119.87 km. The vehicle trajectory and the LDV output are shown in figure 14. The calibration results of different methods in the second experiment are presented in figures 15–17. The DR results of the SINS/LDV integrated navigation system calibrated by different methods are compared in figures 18 and 19 and table 2. The attitude errors and calibration results during calibration without initial alignment are shown in figures 20 and 21. The DR position errors obtained from the calibration results in figure 21 are shown in figure 22.

From figures 15–19 and table 2, it can be seen that the DR position error of LSE-V-KF is smaller than that of SO-KF in the second experiment, while the DR position error of LSE-V-KF is slightly larger than that of SO-KF in the first experiment.
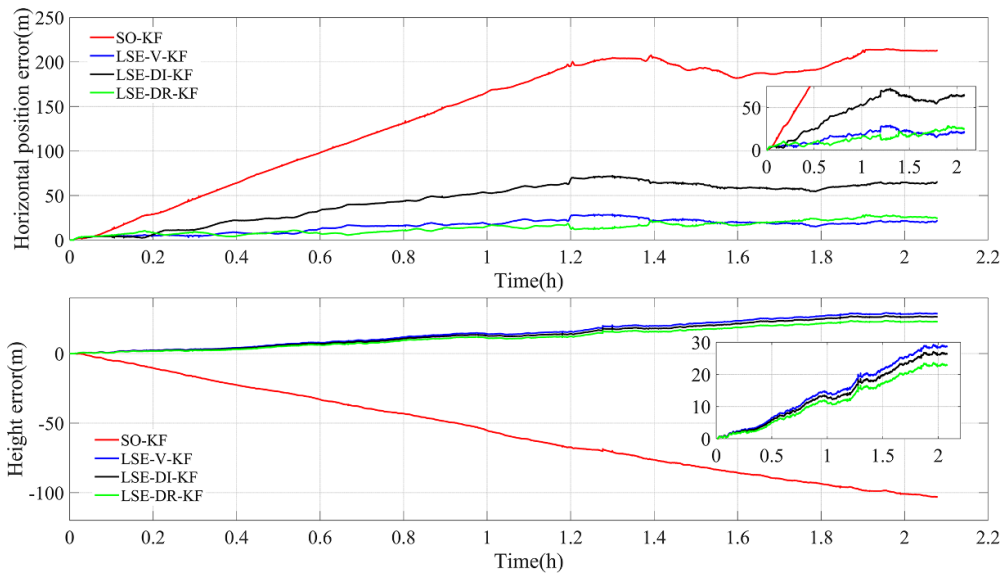
Figure 13. Position error of the first test based on the calibration results of figure 12.
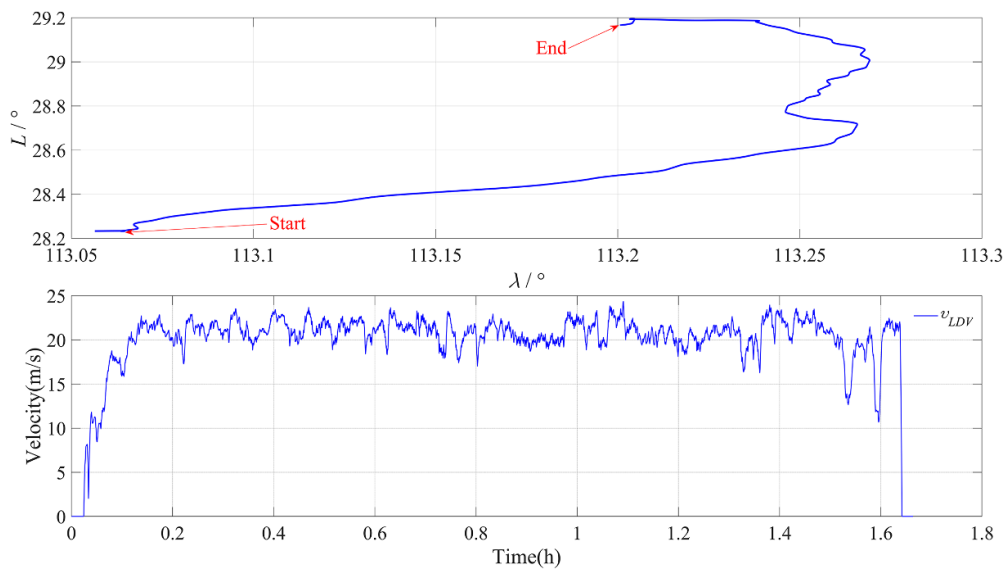
**Figure 14.** Trajectory of the vehicle and velocity curve of the LDV output in the second field test.
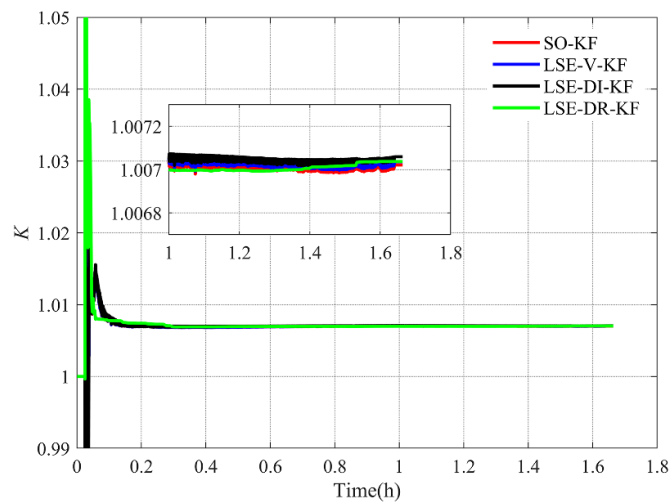
**Figure 15.** Curve of the scale factor in the second vehicle test.

15
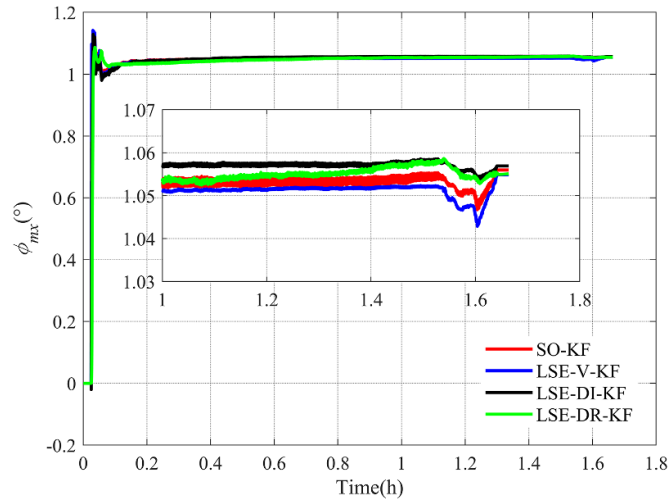
Figure 16. Curve of the pitch misalignment angle in the second vehicle test.
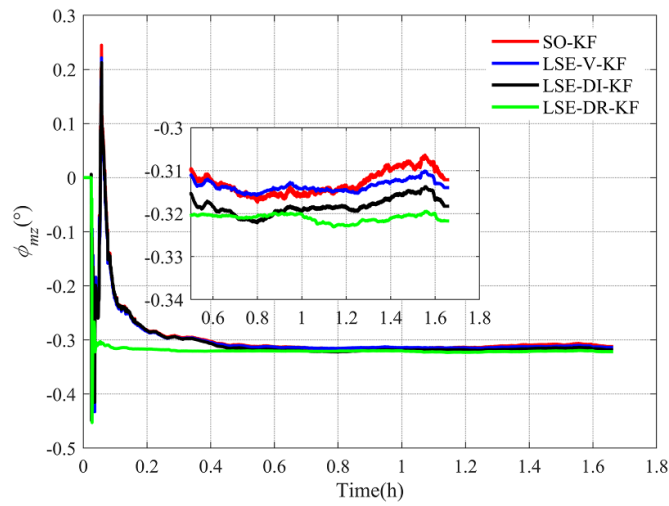
**Figure 17.** Curve of the heading misalignment angle in the second vehicle test.
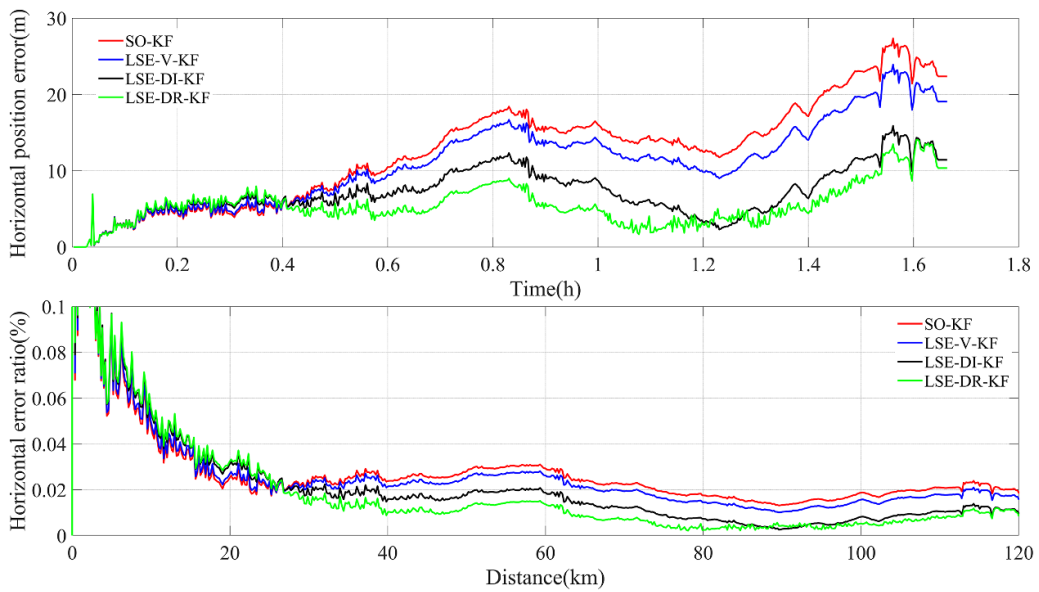
Figure 18. Second test's horizontal location error and horizontal error ratio.

16
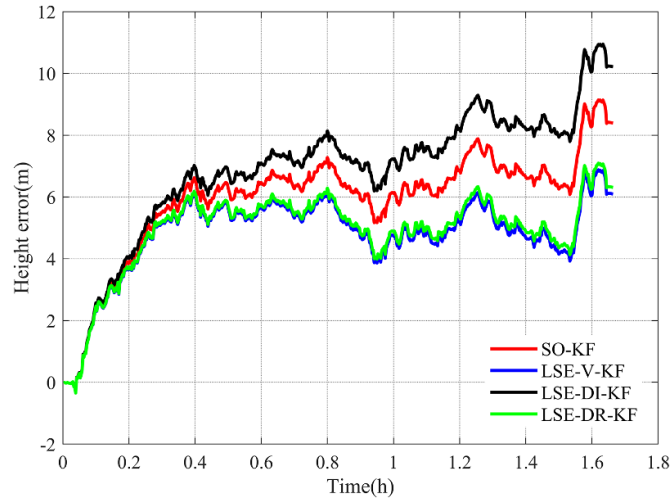
Figure 19. Second test's height positioning error.

Table 2. Performance comparison of the four methods in the second test (119.87 km).

Methods		*Mean* (m)	Error ratio (‰)	*Max* (m)	Error ratio (‰)
SO-KF	Horizontal error	12.66	0.105	27.35	0.228
	Height error	5.93	0.049	9.32	0.078
LSE-V-KF	Horizontal error	11.07	0.092	23.92	0.199
	Height error	4.80	0.040	6.88	0.057
LSE-DI-KF	Horizontal error	7.21	0.060	15.90	0.133
	Height error	6.84	0.057	10.94	0.091
LSE-DR-KF	Horizontal error	5.55	0.046	14.08	0.117
	Height error	4.91	0.041	7.09	0.059
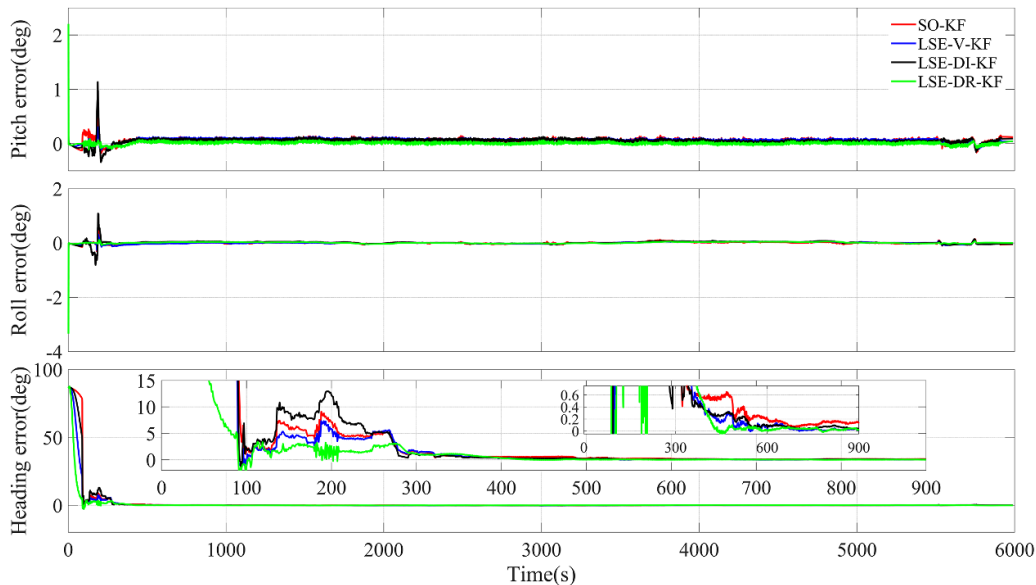
Figure 20. Attitude errors in the second large misalignment test.

This again indicates that LSE-V-KF is not essentially superior over SO-KF, and that under non-harsh conditions, LSE-V-KF and SO-KF have a similar performance. Similarly, the DR horizontal position error of LSE-DR-KF is slightly smaller than that of LSE-DI-KF in the second experiment, indicating that LSE-DR-KF and LSE-DI-KF have similar performance under normal experimental conditions. Consistent with the first experiment, the DR horizontal position errors of
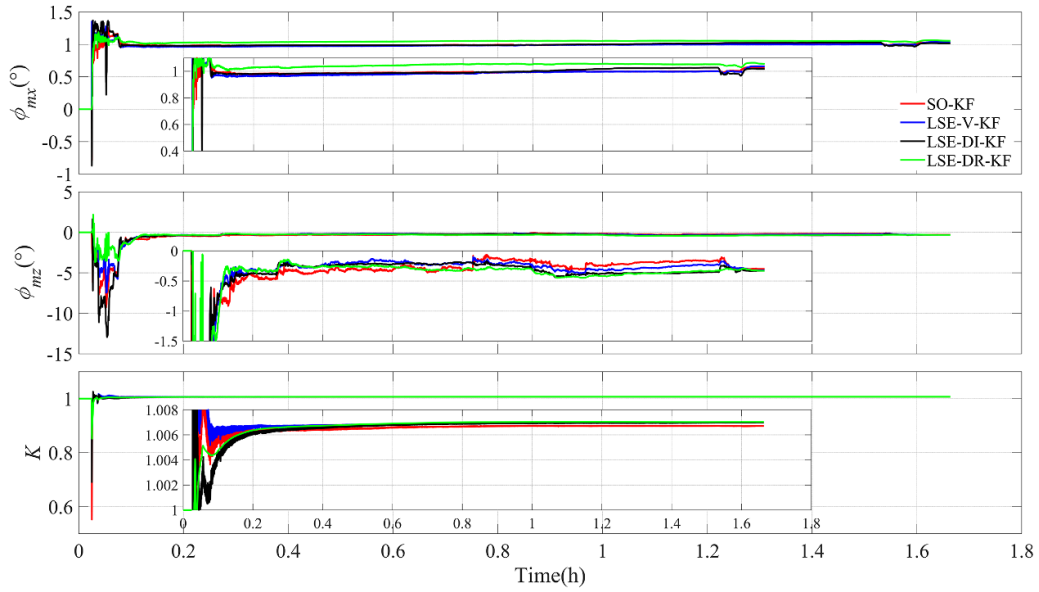
Figure 21. Calibration results in the second large misalignment test.
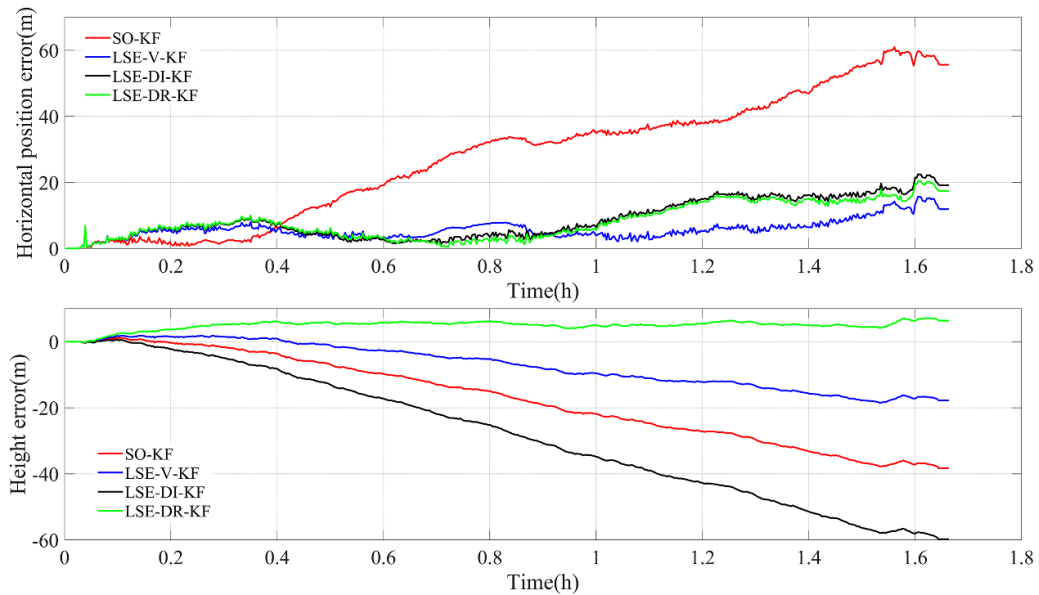
Figure 22. Position error of the first test based on the calibration results of figure 21.

LSE-DR-KF and LSE-DI-KF in the second experiment are still smaller than those of LSE-V-KF and SO-KF, which again indicates that using displacement increment and DR position as the filter observations is helpful to improve the calibration performance. Figure 20 shows that in the second experiment, the heading errors of all four methods without initial alignment converge to within 0.2° within 900 s. However, LSE-DR-KF and LSE-V-KF have better convergence speed and steady-state error than LSE-DI-KF and SO-KF, and SO-KF has the slowest convergence speed and the largest steady-state error. This is consistent with the consistent with the theoretical analysis in sections 3 and 4 as well as the performance of each method shown in the first experiment, so the superiority shown by LSE-DR-KF and LSE-V-KF in figures 21 and 22 is obvious.

6. Conclusion

In this article, the Lie group theory is applied to the traditional calibration method of SINS/LDV integrated navigation system based on Kalman filter, and three online calibration methods based on Lie group left-invariant error model are proposed based on the common observations in integrated navigation, i.e., velocity, displacement increment, and DR position. The effectiveness of the proposed methods is verified by two groups of long-distance vehicle experiments and compared with the traditional calibration method. The results show that under normal conditions (no large attitude misalignment angle and all sensors are working properly), the Lie group -based calibration methods have similar performance

to the traditional calibration method. The calibration results also show that using displacement increment and DR position as the observations improves the calibration performance than using velocity as the observation. To further validate the performance of the proposed method, the calibration performance of the proposed method is tested in the presence of large initial attitude errors, and the results show that the advantage of the Lie group-based calibration method is significant in the presence of large initial attitude misalignment angles. This allows the SINS/LDV integrated navigation system to proceed directly to the calibration process without having to obtain an accurate initial attitude, which can reduce the preparation time for the calibration process. Considering that the IMU used in this paper is a high-precision IMU, the effectiveness of the proposed method will be tested on a low-cost MEMS IMU in future work.

Data availability statements

The data cannot be made publicly available upon publication due to legal restrictions preventing unrestricted public distribution. The data that support the findings of this study are available upon reasonable request from the authors.

Acknowledgments

ORCID iDs

Zhiyi Xiang ● https://orcid.org/0000-0003-1766-2409
Jian Zhou ● https://orcid.org/0000-0001-6443-2644

References

[1] Fu Q, Liu Y, Liu Z, Li S and Guan B 2018 High-accuracy SINS/LDV integration for long-distance land navigation *IEEE/ASME Trans. Mechatronics* **23** 2952–62
[2] Xiang Z, Wang Q, Huang R, Xi C, Nie X and Zhou J 2022 In-motion initial alignment method for a laser Doppler velocimeter-aided strapdown inertial navigation system based on an adaptive unscented quaternion H-infinite filter *Meas. Sci. Technol.* **33** 035001
[3] Xiang Z, Zhang T, Wang Q, Jin S, Nie X, Duan C and Zhou J 2023 A SINS/GNSS/2D-LDV integrated navigation scheme for unmanned ground vehicles *Meas. Sci. Technol.* **34** 125116
[4] Xiang Z, Wang Q, Huang R, Xi C, Nie X and Zhou J 2022 A fast robust in-motion alignment method for laser Doppler velocimeter-aided strapdown inertial navigation system *IEEE Sens. J.* **22** 17254–65
[5] Titterton D H, Weston J L and Weston J L 1997 *Strapdown Inertial Navigation Technology* (Peter Peregrinis Limited)
[6] Jian Z and Xingwu L 2010 Research on laser Doppler velocimeter for vehicle self-contained inertial navigation system *Opt. Laser Technol.* **42** 477–83
[7] Wang M, Cui J, Huang Y, Wu W and Du X 2021 Schmidt ST-EKF for autonomous land vehicle SINS/ODO/LDV integrated navigation *IEEE Trans. Instrum. Meas.* **70** 1–9
[8] Xu B, Wang L, Li S and Zhang J 2020 A novel calibration method of SINS/DVL integration navigation system based on quaternion *IEEE Sens. J.* **20** 1
[9] Troni G and Whitcomb L L 2015 Advances in in situ alignment calibration of Doppler and high/low-end attitude sensors for underwater vehicle navigation: theory and experimental evaluation *J. Field Robot.* **32** 655–74
[10] Zhang X, Yin J, Lin Z and Zhang C 2015 A positioning and orientation method based on the usage of INS and single-beam Lidar *Optik* **126** 3376–81
[11] Yan G 2006 Research on autonomous position and azimuth determining systems for land vehicles (Northwestern Polytechnical University) (in Chinese)
[12] Wu Y, Wu M, Hu X and Hu D 2009 Self-calibration for land navigation using inertial sensors and odometer: observability analysis *AIAA Guidance, Navigation, and Control Conf.* (American Institute of Aeronautics and Astronautics)
[13] Wang Q, Gao C, Zhou J, Wei G, Nie X and Long X 2018 Two-dimensional laser Doppler velocimeter and its integrated navigation with a strapdown inertial navigation system *Appl. Opt.* **57** 3334
[14] Tang K, Wang J, Li W and Wu W 2013 A novel INS and Doppler sensors calibration method for long range underwater vehicle navigation *Sensors* **13** 14583–600
[15] Xi C, Wang Q, Nie X, Huang R, Xiang Z, Zhou J and Jin S 2022 Online calibration technology for a one-dimensional laser Doppler velocimeter based on a strapdown inertial navigation system *Appl. Opt.* **61** 1229
[16] Li L, Sun H, Yang S, Ding X, Wang J, Jiang J, Pu X, Ren C, Hu N and Guo Y 2018 Online calibration and compensation of total odometer error in an integrated system *Measurement* **123** 69–79
[17] Xiang Z, Wang Q, Huang R, Jin S, Nie X and Zhou J 2023 Online calibration method for pitch-independent laser Doppler velocimeter based on improved integrated navigation model *IEEE Trans. Instrum. Meas.* **72** 1–13
[18] Xiang Z, Wang Q, Huang R, Jin S, Nie X and Zhou J 2023 A robust online calibration method for SINS/LDV integrated navigation system based on position observation *IEEE Sens. J.* **24** 1
[19] Zhang G, Xie Y, Yi G, Li X and Wang S 2022 An online calibration algorithm of DVL based on Compass/DVL/USBL integrated navigation system *J. Chin. Inert. Technol.* **30** 589–96
[20] Xiang Z, Wang Q, Huang R, Xi C, Nie X and Zhou J 2021 Position observation-based calibration method for an LDV/SINS integrated navigation system *Appl. Opt.* **60** 7869
[21] Guo Y, Xu B and Wang L 2022 A robust SINS/USBL integrated navigation algorithm based on earth frame and right group error definition *IEEE Trans. Instrum. Meas.* **71** 1–16
[22] Scherzinger B M 1996 Inertial navigator error models for large heading uncertainty *Proc. of Position, Location and Navigation Symp.—PLANS'96* (IEEE) pp 477–84
[23] Wang M, Wu W, Zhou P and He X 2018 State transformation extended Kalman filter for GPS/SINS tightly coupled integration *GPS Solut.* **22** 112
[24] Wang M, Wu W, He X, Li Y and Pan X 2019 Consistent ST-EKF for long distance land vehicle navigation based on SINS/OD integration *IEEE Trans. Veh. Technol.* **68** 10525–34

[25] Luo Y, Guo C and Liu J 2021 Equivariant filtering framework for inertial-integrated navigation *Satell. Navig.* **2** 30

[26] Cui J, Wang M, Wu W and He X 2021 Lie group based nonlinear state errors for MEMS-IMU/GNSS/ magnetometer integrated navigation *J. Navig.* **74** 887–900

[27] Chang L and Luo Y 2022 Log-linear error state model derivation without approximation for INS *IEEE Trans. Aerosp. Electron. Syst.* **59** 1–9

[28] Qian L, Qin F, Li K and Zhu T 2022 Research on the necessity of Lie group strapdown inertial integrated navigation error model based on Euler angle *Sensors* **22** 7742

[29] Du S, Huang Y, Lin B, Qian J and Zhang Y 2022 A Lie group manifold-based nonlinear estimation algorithm and its application to low-accuracy SINS/GNSS integrated navigation *IEEE Trans. Instrum. Meas.* **71** 1–27

[30] Xu B, Guo Y, Guo Y and Wang X 2023 A SE(2)-based transfer alignment for large installation misalignment angle *Measurement* **214** 112784

[31] Chang L, Bian Q, Zuo Y and Zhou Q 2023 SINS/GNSS-integrated navigation based on group affine SINS mechanization in local-level frame *IEEE/ASME Trans. Mechatron.* **28** 1–12

[32] Li K and Li W 2023 The error model based on the special Euclidean group SE(3) of the INS: comparison and extension *Digit. Signal Process.* **132** 103820

[33] Chang L, Di J and Qin F 2022 Inertial-based integration with transformed ins mechanization in earth frame *IEEE/ASME Trans. Mechatronics* **27** 1738–49

[34] Tang H, Xu J, Chang L, Shi W and He H 2023 Invariant error-based integrated solution for SINS/DVL in earth frame: extension and comparison *IEEE Trans. Instrum. Meas.* **72** 1–17

[35] Chang L, Tang H, Hu G and Xu J 2023 SINS/DVL linear initial alignment based on Lie group SE$_3$ (3) *IEEE Trans. Aerosp. Electron. Syst.* **59** 1–17

[36] Nie X and Zhou J 2020 Pitch independent vehicle-based laser Doppler velocimeter *Opt. Lasers Eng.* **131** 106072

[37] Barfoot T D 2017 *State Estimation for Robotics* (Cambridge University Press) (https://doi.org/10.1016/j.robot.2017.11.003)

[38] Barrau A and Bonnabel S 2020 A mathematical framework for IMU error propagation with applications to preintegration *2020 IEEE Int. Conf. on Robotics and Automation (ICRA)* vol 38 (IEEE) pp 5732–8

[39] Luo Y, Guo C, You S, Hu J and Liu J 2021 SE$_2$(3) based extended Kalman filtering and smoothing framework for inertial-integrated navigation (arXiv:2102.12897)

[40] Barrau A 2015 Non-linear state error based extended Kalman filters with applications to navigation (Mines Paristech)